THESIS FOR THE DEGREE OF DOCTOR OF PHILOSOPHY

Numerical Assessment of Cavitation Damage in Fluid Machinery: High-Pressure Fuel Injectors and Water-jet Pumps

Mehmet Özgünoğlu

CHALMERS
UNIVERSITY OF TECHNOLOGY

Department of Department of Mechanics and Maritime Sciences
Chalmers University of Technology
Gothenburg, Sweden, 2025

Numerical Assessment of Cavitation Damage in Fluid Machinery: High-Pressure Fuel Injectors and Water-jet Pumps

Mehmet Özgünoğlu

ISBN 978-91-8103-233-8
Doktorsavhandlingar vid Chalmers tekniska högskola, Ny serie 5691.
ISSN 0346-718X

Department of Mechanics and Maritime Sciences
Chalmers University of Technology
SE-412 96 Gothenburg, Sweden
Phone: +46 (0)31 772 1000
www.chalmers.se

Printed by Chalmers Reproservice
Gothenburg, Sweden, 2025.

Umutsuz durumlar yoktur, umutsuz insanlar vardır.

Mustafa Kemal Atatürk

Abstract

Cavitation erosion poses a significant challenge in high-pressure fuel injectors and water-jet propulsion systems, affecting performance and durability. This thesis presents a numerical investigation into cavitation erosion mechanisms using Computational Fluid Dynamics (CFD) methodologies, incorporating turbulence modeling, cavitation closure models, and erosion prediction techniques.

For high-pressure fuel injectors, both static and dynamic lift conditions were examined. The findings highlight that surface deviations significantly affect vapor collapse dynamics and erosion patterns, emphasizing the importance of incorporating multi-hole simulations and real-world geometries for accurate predictions. Additionally, the study demonstrates that transient needle motion, specifically wobbling effects, alters cavitation-induced pressure loads, influencing erosion distribution. A comparison of thermodynamic models showed that the Perturbed-Chain Statistical Associating Fluid Theory with Compressible Vapor (PC-SAFT&CV) model predicts vapor collapse and erosion localization more accurately than the Tait Equation of State with Incompressible Vapor (Tait&IV) approach.

In water-jet propulsion systems, a RANS-based cavitation erosion assessment framework was developed using the Schnerr-Sauer cavitation model. The study reveals that operating conditions, such as inlet velocity and pressure variations, significantly affect cavitation behavior and erosion risk distribution. While the numerical predictions capture high-risk cavitation collapse regions, RANS-based approaches exhibit limitations in resolving transient cavitation structures.

This research contributes to the development of predictive erosion assessment methodologies for industrial applications. Key contributions include an erosion risk assessment framework applicable to both fuel injectors and water-jet propulsion systems, insights into thermodynamic effects and transient needle motion on cavitation erosion, and the implementation of computationally efficient RANS-based assessment tools.

Keywords: Cavitation erosion, high-pressure fuel injectors, water-jet propulsion, CFD, LES, RANS, needle motion, surface deviations, wobbling motion, thermodynamic effects, durability.

List of Publications

This thesis is based on the following publications:

[Paper 1] Mehmet Özgünoğlu, Gerard Mouokue, Michael Oevermann, Rickard E. Bensow, "Numerical investigation of cavitation erosion in high-pressure fuel injectors in the presence of surface deviations". Fuel, vol. 386 (2025), pp. 134174, doi:10.1016/j.fuel.2024.134174..

[Paper 2] Mehmet Özgünoğlu, Gerard Mouokue, Michael Oevermann, Rickard E. Bensow, "Numerical study of cavitation erosion in high-pressure fuel injector: The role of wobbling motion". 2025, *Under review in Wear.*

[Paper 3] Mehmet Özgünoğlu, Marilia G. J. Vaz, Ioannis Karathanasis, Rickard E. Bensow, Michael Oevermann, Gerard Mouokue, Manolis Gavaises, "Effect of thermodynamic modeling and design variations on cavitation erosion in high-pressure fuel injectors". 2025, *Manuscript.*

[Paper 4] Mehmet Özgünoğlu, Martin Persson, Ammar Saber, Rickard E. Bensow, "Numerical prediction of cavitation erosion in a water-jet propulsion system". 2025, *Under review in Ocean Engineering.*

Acknowledgments

I would like to start by expressing my deepest gratitude to my supervisor, Prof. Rickard E. Bensow, for his continuous support, insightful guidance, and encouragement throughout this research. His deep expertise and critical feedback have significantly shaped both the direction and quality of this work. I am also sincerely thankful to my co-supervisor, Prof. Michael Oevermann, for his technical advice and thoughtful discussions, which have greatly contributed to my development as a researcher. I sincerely appreciate the knowledge and experience that Dr. Mohammad Arabnejad shared with me, enriching my understanding and skills in this field. His willingness to share his insights has been invaluable to my research.

I would like to thank Gabriela for her patience and collaboration during our extensive joint work. Special thanks to Gerard, Martin, Ammar, and the colleagues at Kongsberg Maritime and Woodward L'Orange for their valuable collaboration, particularly on the industrial aspects of this research.

I am grateful to my colleagues and friends at the M2 department for their support. Their humor and joy provided encouragement during challenging times. I am especially thankful to my dear friends Mohsen, Mohammad, Ioli, and Atilla for the many unforgettable moments we shared throughout this journey.

Finally, I would like to express my heartfelt appreciation to my parents, to whom I owe everything, and to my sister, Begüm, and her family, whose support has been unwavering every step of the way. Lastly, I thank my fiancée, Buğçe, for her endless patience, love, and encouragement. This work would not have been possible without the strength, understanding, and belief of those closest to me.

This study was funded by the European Union's Horizon 2020 research and innovation programme through the EDEM project, a Marie Skłodowska-Curie Innovative Training Network (grant agreement No. 861002). The computations were enabled by resources provided by Chalmers e-Commons at Chalmers University of Technology and the National Academic Infrastructure for Supercomputing in Sweden (NAISS), partially funded by the Swedish Research

Council through agreement no. 2022-06725. Simulations were performed on the Vera system at the Chalmers Centre for Computational Science and Engineering (C3SE) and on resources provided by the National Supercomputer Centre (NSC) at Linköping University.

Mehmet Özgünoğlu
Gothenburg, May 2025

Contents

Part I

Thesis Summary

CHAPTER 1

Introduction

This chapter presents an overview of the research on cavitation erosion in fluid machinery, specifically focusing on high-pressure fuel injectors and water-jet propulsion systems. It outlines the motivation for studying cavitation-induced erosion, the role of numerical modeling in predicting erosion-prone areas, and the scope of this thesis. The chapter also provides a review of relevant literature on cavitation erosion assessment and concludes with a summary of the research objectives and thesis structure.

1.1 Motivation and background

Cavitation is a phenomenon that occurs in high-velocity liquid flows when local pressure drops below the vapor pressure, leading to the formation of vapor pockets. These cavities can collapse violently, generating high-pressure shock waves and micro-jets, which may cause significant material damage [1]. This process, known as cavitation erosion, is a major concern in various fluid machinery applications, particularly in high-pressure fuel injectors and marine propulsion systems.

Fuel injectors operate under extreme pressure conditions to ensure precise

fuel atomization and efficient combustion. However, rapid needle movements, complex internal geometries, and transient flow dynamics make them highly susceptible to cavitation. The collapse of cavitation bubbles near solid surfaces results in localized material loss, compromising the injector's durability and performance.

Experimental investigations of cavitation erosion in high-pressure injectors are challenging due to the need for specialized equipment to replicate extreme pressure conditions while maintaining precise control over flow dynamics. On the other hand, the ongoing technological development in computational power makes computational techniques a desirable tool in the design phase of fuel injection systems. However, cavitation erosion assessment via numerical approaches for industrial high-pressure fuel injectors is still challenging since it demands high-cost simulations across a wide range of time and length scales [2]. In addition, a significant challenge lies in the lack of universally valid cavitation models, further complicating the accurate prediction of erosion.

While cavitation erosion is a critical challenge in fuel injectors, it also significantly impacts marine propulsion systems, where high-velocity flows and pressure variations lead to material degradation.

Water-jet propulsion systems are dominant in certain applied marine applications due to their efficiency and superior maneuverability compared to traditional propeller-based propulsion systems [3]. However, cavitation erosion remains a critical concern, leading to material degradation, reduced performance, and higher maintenance costs. The interaction of tip leakage vortices, re-entrant jets, and leading-edge flow separation contributes to cavitation erosion in water-jet pumps, deteriorating impeller surfaces and reducing propulsion efficiency, increasing maintenance costs, and inducing vibrations.

Experimental studies have been instrumental in advancing the understanding of cavitation erosion, particularly in water-jet propulsion systems. High-speed imaging techniques provide direct visualization of cavitation inception and bubble collapses [4]. Paint erosion tests help to identify erosion-prone areas [5], [6], while pressure fluctuation measurements offer insights into cavitation dynamics [7].

However, despite their contributions, experimental methods have several limitations. Spatial resolution constraints make it difficult to directly correlate observed erosion with specific flow structures. Additionally, erosion

typically manifests over extended operational periods, making it challenging to capture its full progression in controlled laboratory settings. Identifying erosion-prone areas at later stages of the design process can lead to costly modifications, emphasizing the need for accurate early-stage prediction methods [5]. Computational Fluid Dynamics (CFD) has become an essential tool for overcoming these limitations by providing detailed simulations of cavitation and cavitation erosion mechanisms.

To address these challenges, numerical modeling has become an essential tool for cavitation erosion assessment in fluid machinery. Extensive research has been conducted to develop computational approaches that enhance erosion prediction and mitigation strategies.

1.2 Numerical cavitation erosion assessment in fluid machinery

Numerical studies of cavitation erosion cover various applications, including propellers, hydrofoils, and hydraulic components. These studies use high-fidelity methods to capture key mechanisms such as vapor collapse, pressure waves, and micro-jet formation [8], [9]. Both Large Eddy Simulation (LES) and Reynolds-Averaged Navier-Stokes (RANS) methods have been widely applied to simulate multiphase flows and turbulence dynamics. For example, Bensow and Bark [10] demonstrated that LES effectively captures reentrant jets and sheet cavity dynamics in propellers, while Li et al. [11] introduced an erosion intensity function derived from unsteady RANS simulations to assess risks on hydrofoil surfaces.

Advanced techniques have further enhanced erosion prediction. These include density-based methods that focus on compressibility effects [12] and micro-jet-based erosion models [13], [14], validated through experimental data. Additionally, methods addressing energy cascading and cavitation intensity, as proposed by Schenke [15] and Arabnejad et al. [16], have improved the understanding of micro-jets and shock waves. These studies collectively demonstrate the potential of numerical models for predicting and mitigating cavitation erosion.

The following sections provide an overview of numerical approaches used in cavitation erosion assessment, focusing on high-pressure fuel injectors and water-jet pumps.

1.2.1 High-pressure fuel injector studies

Numerical assessment of cavitation-induced erosion in fuel injectors can be grouped into the following categories: modeling with density-based and pressure-based solvers, taking into account different turbulence and cavitation closures, and assessment of cavitation-induced erosion with different erosion indicator metrics.

Örley et al. [17] performed LES methodology inside a nine-hole common rail diesel injector during a full injection cycle using a fully compressible flow solver. They also conducted simulations under steady needle lift conditions. Their conclusion is that consideration of the unsteady needle motion is necessary for accurate prediction of erosion sensitive areas.

An explicit density-based approach is applied with real-fluid thermodynamic closure by Kolovos et al. [18]. They used different types of thermodynamic closures with the WALE–LES model and investigated the fuel heating and cavitation erosion location relationship during the needle movement for the five-hole injector. Their simulation results showed good agreement with X-ray-derived surface erosion images. Another compressible simulation was done by Falsafi et al. [19]. They used real geometries and considered the entire injection cycle with time-dependent rail pressure and transient needle movement.

Santos et al. [20] applied LES methodology with the moving mesh technique using ANSYS to investigate cavitation erosion of a gasoline direct injection (GDi) type injector. Having erosion damage images from the injector durability test, they investigated various erosion indicators and concluded that the accumulated erosive power is the most promising indicator for predicting cavitation erosion. Another LES simulation of a diesel injector is presented in Koukouvinis et al. [21]. They simulated two similar injector designs and compared with X-ray CT scans. The pressure peak resulting from vapor collapse was identified as a key indicator for cavitation erosion. The predicted pressure peaks showed good agreement with the observed erosion patterns.

Koukouvinis et al. [22] numerically investigated the high-pressure fuel pump as well. Here, they used a barotropic equation of state with a homogeneous equilibrium model. The locations susceptible to cavitation-induced erosion are identified based on the concept of an adverse pressure gradient, which serves as the necessary cause for the collapse of cavitation structures.

Brunhart [23] studied the predictive capability of different erosion indi-

cators for two fuel injection systems. His motivation was to compare the original eroding design with a modified non-eroding design together with the experimental erosion images. In this benchmark study, DES and RANS turbulence modeling approaches are investigated. Squared material derivative, $(DP/Dt)^2$, and second derivative of potential power density, $PPD2$ [24], were the most promising erosion indicators among the ones investigated.

Cristofaro et al. [25] simulated the generic Spray A case from the Engine Combustion Network (ECN) with the implicit compressible pressure-based and three-phase algorithm. They used the Coherent Structure Model as an LES model for subgrid turbulence. Cavitation erosion prone locations are evaluated by recording the maximum intensity of pressure on the surface. Later, they applied the same algorithm to simulate cavitation in a diesel injector [26]. Here, they particularly investigated the effect of the geometry alterations caused by cavitation erosion by analyzing the nominal design geometry and the eroded one. One of the purposes of their study was to assess cavitation erosion. They concluded that pressure peaks recorded on the nominal geometry correlated well with the experimentally observed erosion regions. Moreover, they applied the same cavitation erosion assessment strategy [27] to the well-reported micro throttle [28].

Zang et al. [29] conducted simulations to investigate the effects of nozzle K-factor, defined as the ratio of the inlet-outlet diameter difference to the nozzle length, and needle lifts on the cavitating flow field and erosion risk within a diesel nozzle featuring a double array of holes. The relative risk of surface erosion served as an index for evaluating cavitation erosion risk on nozzle hole surfaces. The results showed that increasing the K-factor significantly reduced cavitation intensity on hole surfaces, causing cavitation to retract towards the orifice entrance.

Kumar's study [30] evaluates the Zwart-Gerber-Belamri (ZGB) cavitation model coupled with the RANS turbulence model and taking into account the compressibility of both gas and liquid phases. Here, a quantitative and qualitative comparison was conducted against experimental data. Flow field analysis revealed the formation of vortices in the injector sac volume, including *hole-to-hole* connecting vortices and double *counter-rotating* vortices from the needle wall.

Wang et al. [31] investigated the internal flow characteristics and spray patterns of double-layer multi-hole diesel engine injector nozzles. Both exper-

imental and computational approaches were employed to analyze variations between upper and lower layer nozzle holes. Actual geometry derived from X-ray scans facilitated accurate characterization of individual injection holes. Results indicated more intense cavitation development in upper layer holes, leading to higher injection rates and less cycle-to-cycle variations in spray patterns from lower layer holes.

Magnotti's work [32] introduced the Cavitation-Induced Erosion Risk Assessment (CIERA) tool, which connects multiphase flow simulation predictions with material erosion progression. The tool's development involved validating cavitation and erosion predictions for pressurized diesel fuel flow within channel geometries, including variations in Reynolds and cavitation numbers and different inlet corner geometries. The multiphase flow within the channel was modeled using a compressible mixture model with a homogeneous relaxation model for phase change and a dynamic structure approach with LES for turbulent flow. CIERA predictions demonstrated accurate qualitative and quantitative assessment performances when the results are compared with the experiments.

Mariasiu et al. [33] analyzed the impact of different biofuels on erosion during the injection process. They observed varying erosion intensities when using diesel, biodiesel, and vegetable oils. Their findings emphasized the importance of enhancing injection system design and maintenance practices for compression ignition engines fueled with biodiesel.

Mouvanal et al. [34] followed a numerical procedure and aimed at predicting potential erosion caused by cavitation in flow devices such as throttles and nozzles. The proposed technique efficiently captures periodic vapor cloud shedding and collapse, allowing for the prediction of cavitation erosion zones. An algorithm detects collapse pressures indicative of material erosion due to cavitation. Numerical predictions were validated against experimental data, suggesting potential application in reducing the design cycle time of fuel injectors.

Previous studies have explored a variety of erosion metrics, turbulence models, multiphase models, and flow conditions, highlighting the key physical mechanisms such as cavitation cloud implosions and the generation of high-pressure micro-jets. These efforts have provided valuable insights into the detection of erosion-sensitive areas in high-pressure fuel injectors. However, a major limitation of many studies lies in the use of idealized geometries,

which fail to capture the manufacturing deviations present in real-world applications. Realistic geometry modeling plays a pivotal role in accurately simulating cavitation dynamics and erosion patterns. Manufacturing deviations, often overlooked in Computer-Aided Design (CAD) models, can significantly influence cavitation behavior, especially in a high-pressure environment.

To the best of the author's knowledge, no prior studies have directly investigated the specific effects of surface or manufacturing deviations on cavitation and cavitation erosion. This gap is critical because such deviations introduce complex flow interactions that may significantly alter erosion predictions, particularly in high-pressure fuel injector systems. Addressing this gap is essential for advancing cavitation modeling and improving the predictive accuracy of erosion assessments in real-world applications.

In addition to geometry considerations, the choice of numerical methodology significantly impacts the predictive accuracy of cavitation modeling. Reynolds-Averaged Navier-Stokes (RANS) and Large Eddy Simulation (LES) are widely used approaches, each offering distinct advantages. LES captures detailed turbulence structures and provides insights into complex flow phenomena, but its high computational cost often limits its use in industrial applications. RANS, on the other hand, offers a more computationally efficient alternative, though it may lack the fidelity needed to resolve intricate cavitation dynamics.

Lastly, existing transient needle simulations predominantly rely on Large Eddy Simulation (LES) due to its ability to resolve detailed flow structures and cavitation dynamics [17], [18], [21]. However, the high computational cost and time requirements associated with LES limit its applicability in industrial scenarios. Additionally, studies have largely focused on vertical needle lift [19]–[21], [35], neglecting the potential influence of off-axis motion on cavitation erosion. It's important to note that some studies [36]–[42] have explored how three-dimensional (vertical and off-axis) needle movement affects cavitation and spray dynamics. While most of these studies did not explicitly evaluate its impact on cavitation erosion, Devassy et al. [37] conducted such an analysis but using a simplified model. Finally, while advanced techniques such as overset meshing offer the potential to overcome limitations of traditional moving mesh approaches [18], [26], they remain under-explored in the context of transient needle dynamics. These gaps underscore the need for a comprehensive numerical framework that addresses both computational

efficiency and realistic needle motions.

1.2.2 Water-jet pumps studies

For marine propulsors and hydrofoils, various turbulence models have been used for cavitation and cavitation erosion simulations, including Reynolds-Averaged Navier-Stokes (RANS), Detached Eddy Simulation (DES), and Large Eddy Simulation (LES). RANS-based models are commonly used in industrial applications due to their computational efficiency [11], [43]–[46]. However, they often struggle to resolve transient cavitation structures and high-frequency pressure fluctuations, both of which are essential for accurate erosion prediction [47]. DES methods combine RANS modeling near walls with LES in separated flow regions, improving accuracy in complex cavitating flows [48]–[51]. LES models further enhance resolution but require substantial cost, limiting their industrial feasibility [52]. Alternatively, Xu et al. [53] applied wall-modeled LES (WMLES) to study unsteady flow in water-jet pumps. Their study demonstrated the predictive capability of WMLES while also highlighting its significant computational demands.

In addition to turbulence modeling, multiphase cavitation modeling defines how vapor cavities interact with the surrounding liquid phase. Eulerian models approximate cavitation as a homogeneous mixture, where vapor and liquid phases are assumed to move at the same velocity. These models are computationally efficient but often fail to resolve individual bubble collapse behavior, which is critical for erosion prediction [54], [55]. In contrast, Eulerian-Lagrangian models explicitly track individual vapor bubbles, improving predictions of localized collapse pressures, micro-jets, and shock waves [56]–[58].

Most numerical cavitation erosion studies focus on marine propellers and hydrofoils, where erosion is primarily caused by tip vortex cavitation, cloud cavitation, and re-entrant jets. Numerical studies have successfully applied density-based compressible models to resolve collapse-induced impact pressures [59]. Other approaches have introduced micro-jet impact and energy-based models, validated through soft paint erosion tests and ductile material erosion simulations [15], [51], [60], [61]. While these models have significantly improved erosion prediction for propellers, their application to water-jet propulsion systems remains under-explored. However, even with advances in cavitation erosion modeling, existing erosion prediction tools lack the ro-

bustness and efficiency needed for routine industrial use [52]. Most previous studies have focused on a single operating condition, limiting their ability to assess cavitation erosion risk comprehensively.

Unlike marine propellers, most studies on cavitation in water-jet pumps have focused on performance degradation and flow instabilities rather than erosion risk [46], [54], [55], [62]. Previous investigations have examined the effects of non-uniform suction flow and swirl distortion on cavitation inception, showing how secondary flow structures influence cavitation intensity [54]. Other studies have analyzed blade loading variations and demonstrated that different geometries significantly alter cavitation behavior [55]. Arabnejad et al. [63] performed LES simulations of the AxWJ-2 axial water-jet pump, identifying tip leakage vortices as a key factor in cavitation development. Water-jet pumps differ from open marine propellers due to their fully wall-bounded, confined, and complex geometries. These conditions significantly increase computational complexity for high-fidelity CFD methods such as LES and DES, especially in near-wall regions where fine mesh resolution is required [5], [63]. High-fidelity simulations, although accurate, are often impractical due to their high computational demands [47]. Lower-cost alternatives, such as RANS-based models, require further validation to be applied reliably to cavitating flows. The confined, wall-bounded nature of water-jet propulsion systems makes this validation even more critical [5], [52].

Studies specifically assessing cavitation erosion in water-jet pumps remain limited. One of the few examples is Qiu et al. [64], who proposed the Erosive Power Method (EPM), correlating erosion severity with cavitation collapse intensity. Their approach provided a computationally efficient alternative to high-fidelity simulations but required further validation in complex cavitating flows. Arabnejad et al. [5] later investigated erosion risks in a different geometry, applying LES and an erosion model based on energy cascading [16].

Despite significant advancements in cavitation and erosion modeling, several key challenges persist. The aforementioned studies have demonstrated good agreement between numerical erosion risk predictions and experimental observations. However, the robustness of these models across varying operating conditions remains a concern. Many high-fidelity models provide accurate erosion predictions but are often computationally expensive and complex to integrate into industrial design workflows. This poses a major challenge for industrial applications, where computational efficiency is critical for practi-

cal implementation. The trade-off between computational cost and model accuracy continues to be a challenge, as high-fidelity methods such as LES and Eulerian-Lagrangian approaches offer superior resolution but require extensive computational resources. For industrial frameworks, it is essential to develop numerical models that not only provide reliable erosion predictions but also remain computationally feasible for routine engineering design and optimization. Additionally, while cavitation erosion in marine propellers has been extensively studied, the water-jet pumps have received less attention in this regard.

1.3 Objective and Scope of the Thesis

The primary objective of this thesis is to develop and apply a numerical framework for cavitation erosion assessment in fluid machinery, with a focus on high-pressure fuel injectors and water-jet propulsion systems. The research aims to improve the predictive capabilities of cavitation erosion models while maintaining computational efficiency, making them viable for industrial applications. The key objectives of this thesis are:

- Develop and validate a CFD-based erosion assessment methodology applicable to industrial time scales.
- Investigate the influence of modeling choices—turbulence models (RANS/LES), thermodynamic closures, and geometric deviations—on erosion prediction accuracy.
- Analyze the fundamental hydrodynamic mechanisms that contribute to aggressive cavitation collapse.
- Evaluate the effect of system-specific operational and design parameters—such as needle wobbling and geometry variations in fuel injectors, and operating conditions in water-jet propulsion systems—on cavitation erosion behavior.

This thesis is based on four research papers, each contributing to different aspects of cavitation erosion modeling and assessment:

Paper 1 investigates cavitation erosion in high-pressure fuel injectors, focusing on the effect of surface deviations on cavitation behavior. The study

utilizes LES and RANS models to analyze erosion-prone regions and evaluates different erosion indicators to identify the most reliable metric for cavitation-induced material damage. The best-performing erosion indicator from this study is applied in subsequent papers.

Paper 2 extends the investigation to transient needle motion, specifically wobbling effects, to determine how lateral off-axis displacement alters cavitation behavior and erosion risk in high-pressure fuel injectors. Dynamic lift simulations with RANS are used to assess how transient needle motion influences vapor collapse intensity and erosion formation.

Paper 3 investigates the effect of thermodynamic modeling and needle design variations on cavitation erosion prediction in high-pressure fuel injectors. The results highlight the critical role of both thermodynamic fidelity and geometric optimization in improving prediction accuracy and guiding injector design.

Paper 4 shifts the focus to water-jet propulsion systems, developing a computationally efficient RANS-based methodology for cavitation erosion risk assessment. The study evaluates the influence of operating conditions (inlet velocity, pressure fluctuations) on cavitation dynamics and compares numerical predictions with experimental soft paint erosion tests. The findings highlight the limitations of RANS-based modeling in capturing transient cavitation structures while demonstrating its practical use as an early-stage erosion risk assessment tool.

By addressing these objectives, this thesis provides a comprehensive numerical framework for cavitation erosion assessment, balancing predictive accuracy with computational efficiency to support industrial applications.

1.4 Thesis Outline

This thesis is structured into two key parts: a comprehensive summary and a collection of appended research papers.

Part 1: Thesis Summary

The first part of this thesis provides an overview of the research with following chapters:

- **Chapter 1: Introduction**
  This chapter provides an overview of the motivation behind the study, the significance of cavitation erosion in fluid machinery, and the previous

numerical studies. It also defines the research objectives and the scope of the thesis.

- **Chapter 2: Methodology**
  The methodological approach used in this thesis is outlined in this chapter. It details the numerical models for cavitation, turbulence, thermodynamic, and cavitation erosion assessment.

- **Chapter 3: Case Studies**
  This chapter presents the application of numerical methods to specific cases. It covers simulations of cavitation erosion in high-pressure fuel injectors and water-jet propulsion systems, describing operating conditions, computational domains, and experiments.

- **Chapter 4: Summary of Included Papers**
  A summary of the key findings from the papers included in the thesis is presented here.

- **Chapter 5: Concluding Remarks and Future Work**
  The final chapter summarizes the main conclusions drawn from this research and provides recommendations for future investigations in cavitation erosion assessment.

Part 2: Appended Papers

The second part of the thesis consists of the original research papers that provide the foundation for this work.

The appended papers included in this thesis are:

- **Paper 1** – Numerical investigation of cavitation erosion in high-pressure fuel injectors in the presence of surface deviations.

- **Paper 2** – Numerical study of cavitation erosion in high-pressure fuel injectors: The role of wobbling motion.

- **Paper 3** – Effect of thermodynamic modeling and design variations on cavitation erosion in high-pressure fuel injectors.

- **Paper 4** – Numerical prediction of cavitation erosion in a water-jet propulsion system.

CHAPTER 2

Methodology

This chapter describes the numerical approach used to assess cavitation erosion in fluid machinery. It outlines the computational framework, turbulence modeling techniques, cavitation models, thermodynamic modeling, and erosion assessment methodologies.

A summary of the geometries, turbulence models, and thermodynamic models used in the different studies is provided in Figure 2.2 at the end of this chapter.

2.1 Numerical setup

The computational framework in this thesis is based on two commercial solvers:

- Ansys Fluent is used for high-pressure fuel injector simulations (Papers 1–3), employing a pressure-based formulation and the Mixture model for multiphase flow modeling [65].
- Simcenter STAR-CCM+ is used for water-jet pump simulations (Paper 4), utilizing an incompressible cavitating flow approach with the Volume of Fluid (VOF) method [66].

In Ansys Fluent, pressure-velocity coupling was handled using either the Coupled algorithm (Papers 1–2) or the SIMPLE method (Paper 3), depending on the simulation setup. The pressure equation was discretized using either the Body Force Weighted scheme or the PRESTO! scheme. Second-order upwind schemes were used for the momentum, volume fraction, density, and turbulence transport equations to ensure numerical accuracy in regions with steep gradients.

Time integration was performed using either first-order or second-order implicit schemes. In Paper 1, second-order accuracy was used for both RANS and LES cases. In Papers 2 and 3, a first-order scheme was applied due to numerical instability or overset mesh limitations. Adaptive time stepping was employed, with the time step controlled by the Courant number (e.g., CFL $<$ 2 for RANS and $<$ 1 for LES).

In STAR-CCM+, a segregated solver was used to solve the incompressible RANS equations. The VOF method was applied for multiphase modeling, and the HRIC (High-Resolution Interface Capturing) scheme was used for volume fraction discretization. Although HRIC may introduce numerical diffusivity, its use was deemed appropriate given the focus of the analysis.

Convergence was monitored using residual thresholds (typically 10^{-5} or stricter), and physical quantities such as mass transfer rates and erosion indicators were used as supplementary convergence criteria.

Since the governing equations and solver-specific implementations are extensively documented in the literature [65], [66], only the sub-models specific to cavitation and erosion are described in detail in the following sections.

2.1.1 Turbulence modeling

Cavitation is highly sensitive to local pressure fluctuations, which are strongly influenced by turbulence dynamics [1]. Therefore, the selection of an appropriate turbulence model is crucial for accurately capturing cavitation structures and vapor collapse phenomena [67]. In this thesis, two turbulence modeling approaches were employed based on accuracy and computational feasibility: the Reynolds-Averaged Navier-Stokes (RANS) $k{-}\omega$ SST model and the Large Eddy Simulation (LES) WALE model.

The $k-\omega$ SST model was used in Papers 1, 2, and 4 due to its robustness, computational efficiency, and reliable performance in flows with adverse pressure gradients and near-wall regions [68]. To better capture cavitation dy-

namics, especially in vapor-dominated regions, the model was augmented with the viscosity correction proposed by Reboud et al. [69]. This correction limits the eddy viscosity in regions with low density, enhancing the unsteadiness of the solution and enabling more accurate prediction of vapor cloud dynamics. These characteristics make the SST model particularly suitable for simulating industrial configurations such as water-jet pumps and high-pressure fuel injectors under unsteady operating conditions.

For higher-fidelity studies requiring detailed resolution of turbulent flow structures—particularly vapor cloud collapse and transient instabilities—LES with the Wall-Adapting Local Eddy-viscosity (WALE) model was used in Paper 1 for high-pressure fuel injector simulations. The WALE model has been shown to perform well in capturing shear-layer dynamics and near-wall vortex activity, which are critical to accurately predict cavitation-induced erosion [2], [5], [63], [70].

The choice between these turbulence models was guided by the trade-off between computational expense and the level of physical detail needed, as motivated by the simulation objectives and discussed in detail in the appended papers (Papers 1–4).

2.1.1.1 RANS $k-\omega$ SST model

The shear-stress transport $k-\omega$ turbulence model ($k-\omega$ SST) [68] is employed within the unsteady (RANS) formulation. It effectively blends the $k-\omega$ and $k-\epsilon$ models in the regions of near-wall and free-stream, respectively. Hence, robustness and accuracy are provided with the help of blending functions [65].

A special treatment is applied to the turbulent viscosity, μ_t, which was previously proposed by Reboud et al. [69]. It is an *ad hoc* method to reduce eddy viscosity in the mixture to allow for a more dynamic flow behaviour. The correction is expressed as

$$\mu_t = \frac{\rho^{'} k}{\omega} \frac{1}{\max\left[\frac{1}{\alpha^*}, \frac{S\ F_2}{a_1 \omega}\right]}, \tag{2.1}$$

$$\rho^{'} = \rho_v + \frac{(\rho_m - \rho_v)^n}{(\rho_l - \rho_v)^{n-1}}, \tag{2.2}$$

$$\rho_m = \alpha \rho_v + (1-\alpha)\rho_l. \tag{2.3}$$

Here, the proposed density function $\rho^{'}$ returns a value in the mixture, including the corresponding phase contributions. In this way, unrealistically high values of the turbulent viscosity are prevented and an unsteadiness of cavitation is achieved [71]. This correction is applied via User Defined Function (UDF) implementation. This approach has been widely adopted in cavitation studies to ensure physical realism of the modeled flow field in vapor-dominated zones [69], [71].

2.1.1.2 LES WALE model

In the Wall-Adapting Local Eddy-Viscosity (WALE) model [70] the turbulent viscosity, μ_t, is expressed as

$$\mu_t = \rho L_s^2 \frac{\left(S_{ij}^d S_{ij}^d\right)^{3/2}}{\left(\overline{S}_{ij}\overline{S}_{ij}\right)^{5/2} + \left(S_{ij}^d S_{ij}^d\right)^{5/4}}. \tag{2.4}$$

Here, ρ represents the density, L_s denotes the mixing length for subgrid scales, S_{ij}^d is the modified rate-of-strain tensor, S_{ij} corresponds to the resolved rate-of-strain tensor, and $\overline{S}_{ij}$ is the rate-of-strain tensor for the resolved scale. These are given by

$$S_{ij}^d = \frac{1}{2}\left(\overline{g}_{ij}^2 + \overline{g}_{ji}^2\right) - \frac{1}{3}\delta_{ij}\overline{g}_{kk}^2, \tag{2.5}$$

$$\overline{g}_{ij} = \frac{\partial \overline{u}_i}{\partial x_j}, \tag{2.6}$$

$$\overline{S}_{ij} = \frac{1}{2}\left(\frac{\partial \overline{u}_i}{\partial x_j} + \frac{\partial \overline{u}_j}{\partial x_i}\right). \tag{2.7}$$

The mixing length, L_s, in the WALE model is determined using

$$L_s = \min\left(\kappa d, C_w V^{1/3}\right). \tag{2.8}$$

Within this equation, κ represents the von Kármán constant, d is the distance to the closest wall, C_w stands for the WALE constant (with a default value of 0.325), and V denotes the volume of the computational cell.

2.1.2 Cavitation Modeling

In cavitation modeling, the multiphase flow is typically treated as a homogeneous mixture, assuming that the liquid and vapor phases share a common velocity field. This assumption, known as the mixture model, simplifies the governing equations by solving a single set of transport equations for the entire mixture rather than separate equations for each phase.

The continuity equation for the mixture is given by:

$$\frac{\partial}{\partial t}\left(\rho_m\right) + \nabla \cdot \left(\rho_m \overrightarrow{V_m}\right) = 0, \tag{2.9}$$

where ρ_m and $\overrightarrow{V_m}$ are the density and velocity of the mixture, respectively. The mixture properties are computed as volume-fraction-weighted averages of the individual phase properties.

2.1.2.1 Vapor Transport Equation

To model the mass transfer between the liquid and vapor phases, the vapor transport equation is used:

$$\frac{\partial}{\partial t}\left(\alpha\rho_v\right) + \nabla \cdot \left(\alpha\rho_v \overrightarrow{V_v}\right) = R_e - R_c. \tag{2.10}$$

Here, ρ_v is the vapor density, α is the vapor volume fraction, and $\overrightarrow{V_v}$ represents the vapor phase velocity field. R_e and R_c are the mass transfer source terms, which represent evaporation and condensation.

2.1.2.2 Zwart-Gerber-Belamri Model

The Zwart-Gerber-Belamri (ZGB) model is selected to model mass transfer. The ZGB model uses the following rates of mass transfer, first described by Zwart et al. [72]:

$$p < p_v: \qquad R_e = F_v \frac{3\alpha_{nuc}\left(1-\alpha_v\right)\rho_v}{R_b}\sqrt{\frac{2}{3}\frac{p_v - p}{\rho_l}}, \quad R_c = 0, \tag{2.11}$$

$$p \geq p_v : \qquad R_c = -F_c \frac{3\alpha_{nuc}\ \alpha_v\ \rho_v}{R_b} \sqrt{\frac{2}{3}\frac{p - p_v}{\rho_l}}, \quad R_e = 0. \tag{2.12}$$

The mass transfer rate constants are provided in Table 2.1. To assess the influence of ZGB parameters on cavitation dynamics, a sensitivity analysis was conducted by systematically varying the evaporation (F_v) and condensation (F_c) coefficients. The goal of this study was to evaluate how these coefficients influence key aspects of cavitation behavior, such as the spatial distribution of collapse pressures and the extent of cavitation-induced erosion. Specifically, both coefficients were increased to 10 times their default values, and the resulting impact on the phase-change dynamics was examined.

Metrics such as the maximum pressure and the minimum absolute pressure in the flow field were used to assess the performance of these configurations. The sensitivity analysis revealed that increasing the ZGB coefficients enhances the mass transfer rate, aligning the model more closely with thermodynamic equilibrium conditions. This resulted in improved correlation with experimental erosion patterns. This model has been used to model cavitation dynamics in high-pressure fuel injector simulations.

Table 2.1: ZGB Mass transfer coefficients.

Description of the coefficient	**Numerical value**
R_b: Bubble radius [m]	1×10^{-6}
α_{nuc}: Nucleation site volume fraction	5×10^{-4}
F_v: Evaporation coefficient	500
F_c: Condensation coefficient	0.1
P_v: Vaporization pressure [Pa]	6000

2.1.2.3 Schnerr-Sauer model

The Schnerr-Sauer cavitation model describes liquid-vapor phase transitions, modeling mass transfer by considering numerous small bubbles undergoing pressure-dependent phase changes [73]. The mass transfer rate between the liquid and vapor phases is defined as:

$$p < p_v : \quad R_e = C_v \rho_l \frac{3\alpha_v(1-\alpha_v)}{R_b}\sqrt{\frac{2}{3}\frac{p_v - p}{\rho_l}}, \quad R_c = 0 \tag{2.13}$$

$$p \geq p_v : \quad R_c = -C_c \rho_l \frac{3\alpha_v(1-\alpha_v)}{R_b}\sqrt{\frac{2}{3}\frac{p - p_v}{\rho_l}}, \quad R_e = 0 \tag{2.14}$$

where R_e and R_c are the evaporation and condensation mass transfer rates [kg/s], and the vaporization and condensation coefficients, C_v and C_c, are both set to 1.0. The vapor volume fraction is represented by α_v, and the bubble radius, R_b, is assumed to be 1.0×10^{-6} m. The local pressure is denoted as p, and the saturation pressure is set to $p_v = 2065$ Pa. To improve stability and computational efficiency, the model neglects surface tension and slip velocity between the phases.

This model was utilized to model the cavitation dynamics in water-jet pump simulations.

2.1.3 Thermodynamic modeling

This section describes the three different thermodynamic modeling approaches used across the simulations in this thesis. Each model differs in how it treats compressibility effects in the liquid and vapor phases. The selection of each model was based on the target application and the desired balance between accuracy and computational cost.

The Tait equation of state (EOS) with an incompressible vapor assumption was applied in high-pressure fuel injector simulations for Paper 1, Paper 2, and partially in Paper 3. To improve thermodynamic fidelity, Paper 3 also employed the PC-SAFT EOS with a compressible vapor model, enabling a more detailed exploration of cavitation behavior under high-pressure, real-fluid conditions. For the simulations of the water-jet propulsion system in Paper 4, an incompressible mixture model was used, with constant density and viscosity properties for all phases (water, vapor, and air).

2.1.3.1 Tait EOS liquid & Incompressible vapor mixture

The first approach models diesel as a compressible liquid using the Tait EOS, which provides a barotropic formulation to prevent nonphysical pressure spikes at high pressures. This approach simplifies the liquid phase representation

while ensuring numerical stability. The governing equations are given as follows [65]:

$$\left(\frac{\rho}{\rho_0}\right)^n = \frac{K}{K_0}, \tag{2.15}$$

$$K = K_0 + n\Delta p, \tag{2.16}$$

$$\Delta p = p - p_0. \tag{2.17}$$

Relevant description of the parameters and values are given in Table 2.2. Diesel vapor is modeled as an incompressible fluid with physical properties given in Table 2.3 below. Although the vapor phase is incompressible, the mixture can still be considered as compressible [74].

Table 2.2: Diesel liquid properties.

Description	Value
p_0 = reference pressure [Pa]	0
ρ_0 = reference density [kg/m^3]	771.13
K_0 = reference bulk modulus [Pa]	8.179023×10^8
n = density exponent	7.15

Table 2.3: Diesel vapor properties.

Description	Value
Density [kg/m^3]	0.89457
Viscosity [kg/(ms)]	8×10^{-6}

2.1.3.2 PC-SAFT EOS liquid & Compressible vapor mixture

The thermodynamic properties of the liquid phase were determined using the Perturbed-Chain Statistical Associating Fluid Theory (PC-SAFT) equation of state (EoS) [75]. This approach enables the definition of thermodynamic properties based on the residual Helmholtz energy and its derivatives, offering an accurate representation of phase behavior. The transport properties, such as dynamic viscosity and thermal conductivity, were estimated using the residual entropy scaling method [76], [77].

For the vapor phase, the thermodynamic properties were derived using the NIST REFPROP database [78], which accounts for compressibility effects. To enhance computational efficiency, a lookup table approach was employed, wherein the thermodynamic and transport properties of the fuel were precomputed and stored prior to the CFD simulations. This decoupling of property evaluations from the flow calculations significantly accelerated the simulation process [79].

2.1.3.3 Incompressible mixture

All phases are treated as incompressible. The densities of liquid water (ρ_l), vapor (ρ_v), and air (ρ_a) are 998.2, 0.59, and 1.18 [kg/m^3], respectively. Their dynamic viscosity values are 1.1386×10^{-3}, 1.26×10^{-5}, and 1.85×10^{-5} [Pa·s], respectively.

2.1.4 Cavitation erosion assessment

To examine the effect of the cavitation erosion, four variables are tracked in each time step. These variables are pressure (P), material derivative of pressure divided by cell volume $(DP/Dt)/V_{cell}$, square of material derivative of pressure $(DP/Dt)^2$ and second derivative of potential power density ($PPD2$). For the effective analysis of these variables, a User-Defined Function (UDF) implementing two algorithms, MAX1 and MAX2, is utilized. The MAX1 algorithm focuses on identifying the maximum value of the tracked parameters, providing a simplified yet insightful view into the peak conditions that may lead to erosion. Conversely, the MAX2 algorithm offers a more nuanced approach, considering the prevention of the fake collapses due to the surrounding cells and applying specific criteria to identify potential cavitation collapse cells [34], [80]. This dual-algorithm approach enables a robust examination of cavitation phenomena, offering insights into both the instantaneous and evolving conditions that contribute to erosion.

2.1.4.1 Tracked variables

The following four indicators are tracked during the simulations:

1. Pressure (scaled with V_{cell}/V_{ref}): This variable represents the pressure within the system, scaled with the ratio of the cell volume to a refer-

ence volume (V_{ref}). The scaling is performed to eliminate the linear dependency of maximum pressure on the local cell size, as suggested by [2]. This approach ensures that the pressure values are independent of grid resolution, enabling consistent comparisons across simulations with varying mesh configurations.

The reference volume V_{ref} is defined as the smallest cell volume in the computational domain. This choice ensures a stable and consistent scaling factor across the domain, particularly when refining the mesh or performing grid sensitivity studies. While V_{ref} is somewhat arbitrary, it remains constant for all simulations in this study, ensuring that relative comparisons of erosion metrics are unaffected by changes in mesh resolution. It should be noted that altering V_{ref} would proportionally change the scaled pressure values. Therefore, care has been taken to keep this reference volume consistent across all design iterations and configurations, as highlighted in [34].

2. $(DP/Dt)/V_{cell}$: This variable quantifies the material derivative of pressure divided by the cell volume itself. The material derivative provides insights into the rate of change of pressure over time, offering valuable information about the occurrence and intensity of cavitation erosion. The material derivative is defined as

$$\frac{DP}{Dt} = \frac{\partial P}{\partial t} + U \cdot \nabla P. \tag{2.18}$$

3. $(DP/Dt)^2$: This variable represents the square of the material derivative of pressure, reflecting the magnitude of pressure fluctuations. Monitoring the squared material derivative helps us understand the intensity and rapid changes in pressure, which are linked to cavitation erosion.

4. $PPD2$: It measures the second derivative of potential power density, indicating the rate of change of power density with respect to pressure. This variable provides insights into the energy transfer and potential for damage caused by cavitation erosion and is given by [24]

$$PPD2 = (p_v - P)\,\frac{\rho}{\rho_l - \rho_v}\nabla \cdot \mathbf{U} \quad . \tag{2.19}$$

It should be noted that the choice of scaling applied to each indicator varies.

The pressure indicator is scaled with V_{cell}/V_{ref} to eliminate its sensitivity to grid resolution, following the rationale discussed by Schmidt et al. [2] and Mouvanal et al. [34].

The remaining indicators — $(DP/Dt)/V_{cell}$, $(DP/Dt)^2$, and $PPD2$ — are adopted from the benchmarking work of Brunhart [23], who evaluated a broad range of erosion indicators and identified these as the most promising in terms of predictive accuracy. Among these, $(DP/Dt)/V_{cell}$ was shown to benefit from volume scaling and is therefore used in that form. In contrast, no volume-based scaling was specifically investigated for $(DP/Dt)^2$ and $PPD2$ in Brunhart's study. Preliminary tests in this thesis revealed no consistent improvements when volume scaling was applied to these indicators. As such, they are retained in their original unscaled form.

2.1.4.2 Tracking methodologies: MAX1 and MAX2 algorithm

There are two sets of algorithms, MAX1 and MAX2, implemented. The MAX1 algorithm is studied by previous researchers [21], [23]. For this, only the maximum value of the tracked parameter (Table 2.4) is considered. The MAX2 algorithm relies on a prevent mechanism of fake collapses. The idea has been first introduced by Mihatsch et al. [80] and has been reformulated by Mouvanal [34]. Both of the algorithms loop over all cells at the end of each time step.

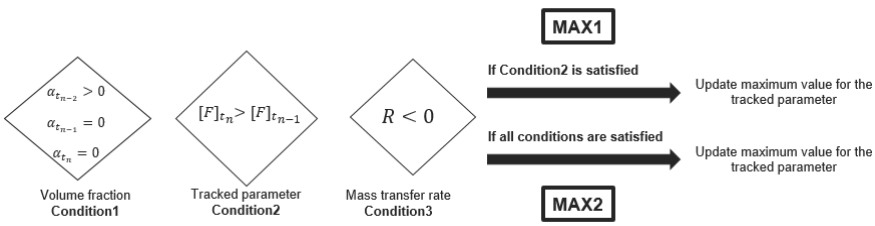

Figure 2.1: MAX1 and MAX2 algorithms.

In particular for the MAX2 algorithm, there are 3 conditions that need to be satisfied to determine the cell as the "collapse cell". These conditions are shown in Figure 2.1.

The first condition is necessary to distinguish whether there are transported

Table 2.4: Description of the variables in MAX1/MAX2 algorithm.

Description	Value
Tracked parameter at current time step	F_{t_n}
Tracked parameter at previous time step	$F_{t_{n-1}}$
Volume fraction of current time step	$\alpha_{t_{n-}}$
Volume fraction of previous time step	$\alpha_{t_{n-1}}$
Volume fraction of two previous time step	$\alpha_{t_{n-2}}$
Mass transfer rate at current time step	R_{t_n}

vapor clouds from neighbouring cells or if they are generated locally. Moreover, collapse due to rebound is particularly examined with a zero vapor volume fraction . This procedure has been first used by Mihatsch et al. [80] with a density-based solver. The second condition is checking the tracked parameter value of the current time step with the previous time step, with the physical insight that a collapse will occur with a higher tracked parameter value. Mouvanal [34] set this tracked parameter as pressure solely. In this study, additional tracked parameters ($(DP/Dt)/V_{cell}$, $(DP/Dt)^2$ and $(PPD2)$) are introduced alongside with the pressure (P). Finally, the third condition ensures that a condensation happened in that cell. Once these 3 conditions are satisfied in that loop, the maximum value for the each tracked parameter is updated within a cell loop that works at the end of each time step.

Paper	Geometry	Turbulence model	Thermodynamic model
Paper1	Static high lift / CAD Model / 1hole	RANS	Tait EOS diesel liquid & Incompressible diesel vapor
	Static high lift / CAD Model / 1hole	LES	
	Static high lift / TS Model / 1hole	RANS	
	Static high lift / TS Model / 1hole	LES	
	Static high lift / TS Model / 8hole	RANS	
Paper2	Static low lift / TS Model / 8hole	RANS	Tait EOS diesel liquid & Incompressible diesel vapor
	Lift only motion / TS Model / 8hole		
	Wobbling motion / TS Model / 8hole		
Paper3	Static low lift / CAD Model /1hole (Validation case)	RANS	Tait EOS diesel liquid & Incompressible diesel vapor
	Static low lift / CAD Model / 1hole (Validation case)		PC-SAFT EOS diesel liquid & Compressible diesel vapor
	Base design		
	NV-01 design		
	NV-02 design		
Paper4	Water-jet pump / Case#1	RANS	Incompressible water, vapor and air
	Water-jet pump / Case#2		
	Water-jet pump / Case#3		

Figure 2.2: Summary of the geometries and models used in the papers.

CHAPTER 3

Case Studies

This chapter presents the numerical case studies conducted in this research. Section 3.1 introduces the high-pressure fuel injector simulations. First, the experimental setup and operating conditions are presented, followed by a description of the geometries, computational domains, and boundary conditions used in the simulations.

Section 3.2 introduces the water-jet propulsion system simulations. Similar to the previous section, the experimental setup and operating conditions are first described, followed by the details of the computational domain and boundary conditions.

3.1 High-pressure fuel injector simulations

This work is described in more detail in Paper 1 and Paper 2, where the related methodology and results are presented. Paper 3 is currently in progress and will provide additional insights once completed.

3.1.1 Operating conditions and experiment

Experiments were performed on a high-pressure injector from Woodward L'Orange, typically used in heavy-duty and marine engines. This injector operates under a pressure of 2200 bar, and features 8 holes designed for optimum fuel delivery. The experiments, conducted at L'Orange facilities, are available for two static lift conditions, 480 µm – high lift and 20 µm – low lift.

Figure 3.9 shows photographs taken at the end of the high lift experiment. The geometry was filled with epoxy material to highlight the gaps caused by erosion, making the eroded regions clearly visible. The experimental images suggest that material removal occurs predominantly on the upper side of the injector holes. However, it's important to note that the bottom side of the injector was not captured clearly in the photographs.

For the low lift experiment, the needle surface damage and sac surface damage are both depicted in Figure 3.2, but using different methods of representation. The needle surface damage is directly visible in the images due to the wear, while the sac surface damage is identified using an epoxy filling technique. Four nozzles were used for the experiment, each corresponding to a different total test duration. The experimental duration for each test is indicated in the middle of the figure, showing successive times of 2, 4.5, 16, and 40 hours from left to right. For both the needle and the sac, erosion patterns gradually increase over time, with the damaged region expanding upstream as erosion progresses. Among the time instants, the 2-hour interval is most suitable for validation as it represents the incubation phase where material removal remains minimal. However, subsequent time instants such as 4.5 and 16 hours offer valuable insights into the progression of erosion patterns for qualitative comparisons.

Although the experiments were conducted at fixed lift positions, erosion patterns varied between injector hole entrances and the needle surface, particularly in the high lift experiment. The needle damage was non-axisymmetric, likely due to misalignment caused by vibrations and/or incorrect positioning. Additionally, surface deviations were a significant factor contributing to these differences.

In the low lift experiment, multiple nozzles were used, each corresponding to a different experimental duration. This introduced subtle geometric variations across the tests, further complicating direct comparisons. The evolving flow field due to material removal also plays a critical role in erosion progression.

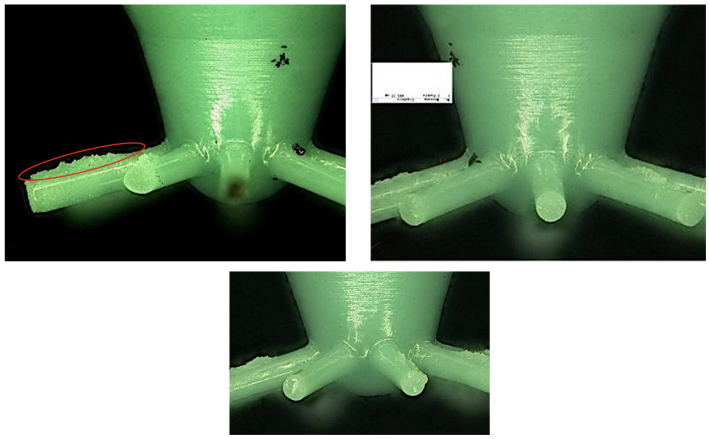

Figure 3.1: Experimental images for the high lift condition (480 µm).

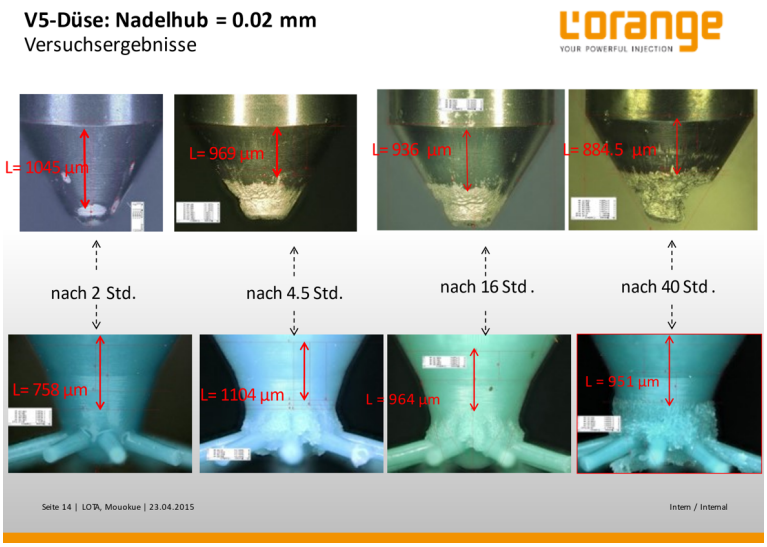

Figure 3.2: Experimental image for the static low lift condition (20 µm).

Finally, while evaluating cavitation erosion experiments, it is important to note that the initial geometry becomes invalid as material removal begins. Therefore, it is crucial to exercise caution when comparing computational fluid dynamics (CFD) results with experimental results, as there are no geometry changes that occur during the calculations. These factors highlight the complexity of correlating numerical predictions with experimental observations.

3.1.2 Geometry and computational domain

3.1.2.1 Static high lift simulations

Geometry modeling is an important phase for CFD simulations. The Computed Aided-Design (CAD) models offer design flexibility and simplification but may not capture real-world physics, while the Tomography Scan (TS) models provide a high-fidelity representation with details of the actual manufactured geometry. Both the CAD and TS models are provided by Woodward L'Orange. The models are represented in Figure 3.3, and include 8 holes as the default configuration. It is clear from the provided figure that the surface deviations are especially noticeable in the injector orifice holes, which are prone to cavitation erosion in the high lift condition.

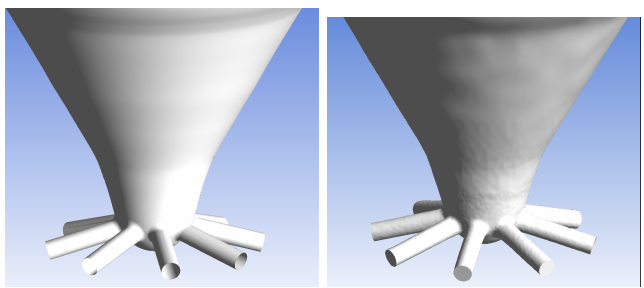

Figure 3.3: CAD model (left) and TS model (right) comparison.

The numerical simulations are first divided into two main categories: CAD model and TS model. These simulations aim to provide a comprehensive understanding of the differences in cavitation erosion behavior in the presence of surface deviations. Computational domains are generated as 1-hole for the CAD model (Figure 3.4c), while for the TS model both 8-hole (Figure 3.4a)

and 1-hole (Figure 3.4b) domains are generated. The purpose of the 8-hole simulations of the TS model is to examine the cavitation erosion performance of each orifice individually, investigate differences between the orifices, and check for interactions between holes.

Considering the cost and time requirements, LES has been employed only for 1-hole computational domains. To provide a consistent comparison with LES simulations, the same computational domains are also analyzed with the RANS approach.

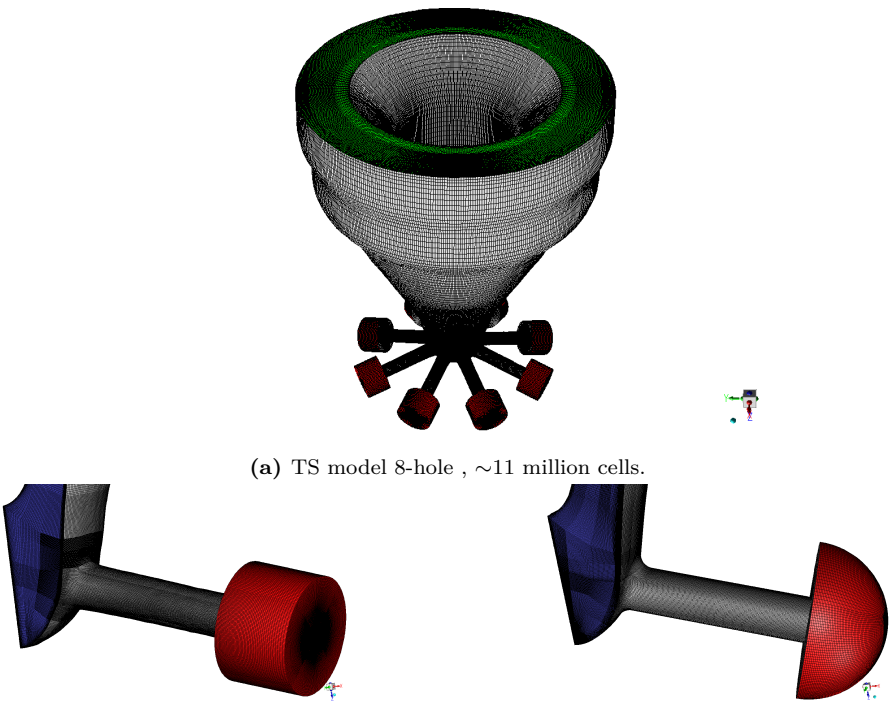

(a) TS model 8-hole , ∼11 million cells.

(b) TS model 1-hole , ∼9 million cells.

(c) CAD model 1-hole , ∼5 million cells.

Figure 3.4: Computational domains with their cell count.

Figure 3.5 presents the surface deviation of the TS model compared to the CAD model when both models in Figure 3.3 are overlapped and aligned in

the center. These contour plots are generated with the GOM Inspect 2022 software [81]. The focus was on analyzing surface deviations, particularly in relation to the orifices' entry dimensions and top/bottom downstream sections.

In general, the top side of the orifices exhibited a positive deviation, while the bottom side showed a negative deviation. These dimensional properties play a crucial role in the generation of cavitation, making this observation particularly significant. The examination further indicated that the entrance diameters of the orifices deviated up to 0.02 mm, positively on the top side and negatively on the bottom side. It is also clear to see that each orifice has different surface deviations and orifice entrance dimensions when they are compared with each other. This is another motivation to analyze TS model with 8-hole configuration using the RANS approach.

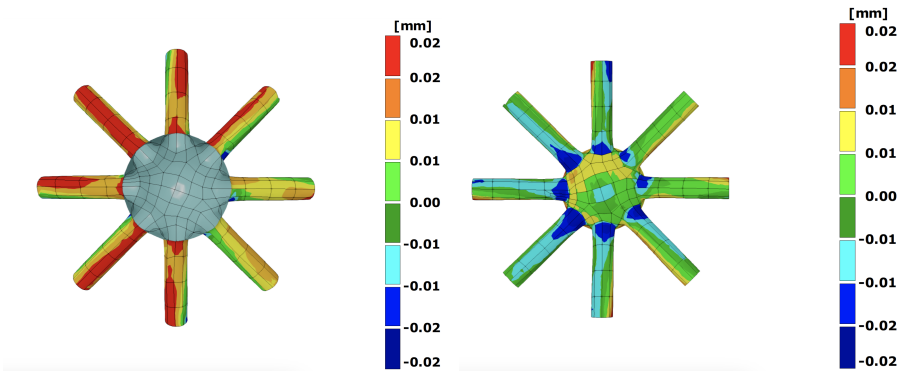

Figure 3.5: Surface deviations between TS and CAD model injector holes. Top view (left), Bottom view (right).

Figure 3.6 illustrates the selected 1-hole, providing a top view of the TS model 8-hole geometry with hole numbering, and a bottom view from the geometry modeler. The upstream seating surfaces exhibit surface deviations, making it more challenging to maintain consistent topology and mesh periodicity. Therefore, 'hole7' was chosen as it presents fewer issues compared to the other holes.

The computational grid should have sufficient quality due to the spatial resolution requirement of LES. While several methods exist to assess grid quality for LES [82], [83], these are typically used for non-cavitating flows. Celik's Index Quality [84] provides a more suitable measure for cavitating LES simu-

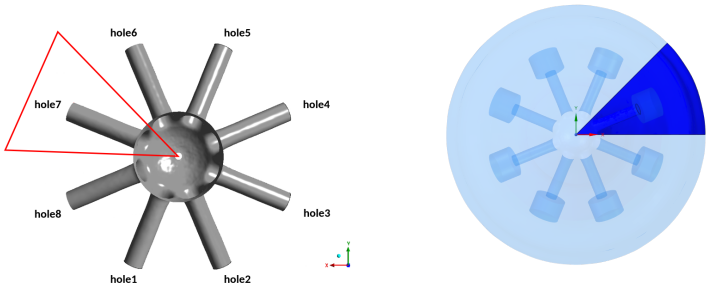

Figure 3.6: Selected hole representation with top and bottom view to the TS model 8-hole geometry.

lations because it accounts for multi-phase effects by having the information of the laminar mixture viscosity (μ) and turbulent mixture viscosity (μ_t). In this study, both Celik's Index Quality and Taylor length scale calculation are both used for the assessment of grid. It is suggested that by Celik et al. [84] that $LESIQ_v$ of 75% to 85% can be considered adequate for most engineering applications, where

$$LESIQ_v = \frac{1}{1 + 0.05\left(\frac{\mu+\mu_t}{\mu}\right)^{0.053}}. \tag{3.1}$$

The above equation is used as a post processing parameter to asses the quality of the grid. So, the computational grid has been analysed (Figure 3.7) both globally and locally with several cut planes via the $LESIQ_v$ parameter. It can be seen from the Figure 3.7 that the global minimum $LESIQ_v$ value is ∼0.81, which lies within the acceptable range (75% to 85%) for LES as suggested by Celik et al [84]. This indicates that the grid quality is sufficient for LES simulations.

The Taylor length scale, calculated using the equation $\lambda_g = \sqrt{10}\mathrm{Re}^{-0.5}L$, was taken into account for mesh refinement in different regions of the injector. The characteristic length, L, represents the relevant physical dimension of each region, such as the orifice diameter, needle seat distance, and average length of the sac volume, which are critical for scaling flow properties. The velocities listed in Table 3.1 are the time-averaged velocities within each specific region. These mean velocities are used to calculate Reynolds numbers and Taylor

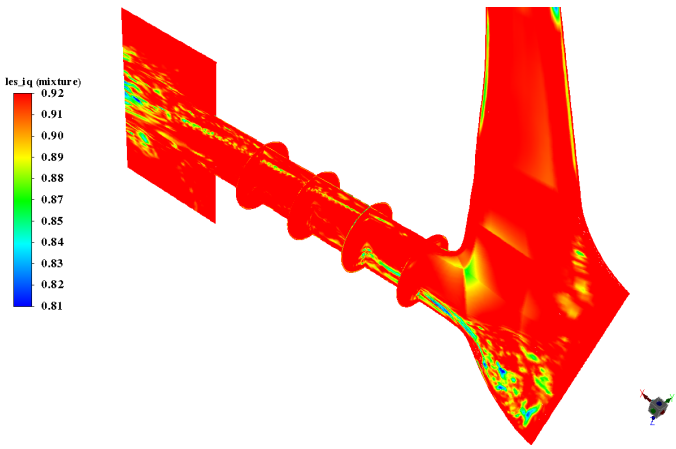

Figure 3.7: Assessment of the grid (TS model 1-hole) with $LESIQ_v$ in various cut planes.

length scale across different injector zones. The values, as shown in Table 3.1, indicate the extent of refinement needed to capture the essential flow dynamics within each region, namely the needle seat, sac volume, and orifice.

Table 3.1: High lift condition.

	Characteristic Length (m)	**Velocity (m/s)**	**Reynolds Number**	**Taylor Length Scale (m)**
Needle Seat	4.8×10^{-6}	200	35000	5×10^{-6}
Sac Volume	~ 0.0008	200	55000	4×10^{-6}
Orifice	0.0003	700	70000	3×10^{-6}

Flow through the geometry is driven via pressure boundary conditions with a purpose of matching experimental conditions. 2200 bar total pressure is set at the inlet, which behaves like a subsonic reservoir boundary condition. Fluctuating velocity at the inlet is not considered, since it does not have any effect on the overall flow field [85]. 10 bar static pressure is given at the outlet surface. It should be noted that the computational domain is extended from the orifice exit to a slightly more downstream position, and outlet ports located at the end of this extension. This extension aims to mitigate the

impact of outlet pressure on the upstream flow field. Additionally, during the simulations, cavitation formations have been observed reaching up to the orifice exit.

To reduce the computational cost, the 1/8 portion of the entire injection system is modeled for 1-hole only simulations. Periodicity is provided with periodic boundary conditions that are applied on the side surfaces. Boundary conditions are also represented with different colours in Figure 3.4.

3.1.2.2 Static low lift simulations

The static low lift simulations were performed to investigate cavitation behavior under low needle lift conditions. Four different injector geometries were considered in this study: the validation case, base design, NV-01 design, and NV-02 design. These geometries, along with their computational domains, are illustrated in Figure 3.8. The validation case consists of approximately 6.5 million computational cells, whereas the base, NV-01, and NV-02 designs have around 3.8 million cells each. The fully hexahedral meshing strategy ensured that regions prone to cavitation were well resolved while maintaining computational efficiency.

The primary objective of the validation case was to assess the performance of different thermodynamic models in predicting cavitation behavior. Two distinct thermodynamic approaches were tested: the *Tait EOS diesel liquid & Incompressible diesel vapor* and the *PC-SAFT EOS diesel liquid & Compressible diesel vapor*. These numerical predictions were compared against low lift experimental data from Section 3.1.1 to evaluate their numerical erosion assessment accuracy.

Following the validation study, the cavitation erosion assessment was conducted for the alternative needle designs, including the base, NV-01, and NV-02 configurations. These simulations were performed using the *PC-SAFT EOS diesel liquid & Compressible diesel vapor* mixture. The erosion-prone regions and cavitation structures were analyzed to understand the impact of the needle design modifications on cavitation intensity and potential material damage.

The validation case was simulated with an inlet pressure of 2200 bar and an outlet pressure of 20 bar. Although the experimental conditions in Section 3.1.1 specify an outlet pressure of 10 bar, this setting led to numerical instabilities in the simulations. To ensure computational stability while main-

taining physically meaningful results, the outlet pressure was increased to 20 bar.

The base, NV-01, and NV-02 designs were tested under different thermodynamic conditions to simulate realistic injection scenarios. In these cases, the inlet pressure was set to 1600 bar with a temperature of 90 K, while the outlet conditions were maintained at 50 bar and 780 K. Since the NV-01 and NV-02 geometries are modified versions of the base design, they were simulated under the same operating conditions to isolate the effects of geometric modifications on cavitation behavior.

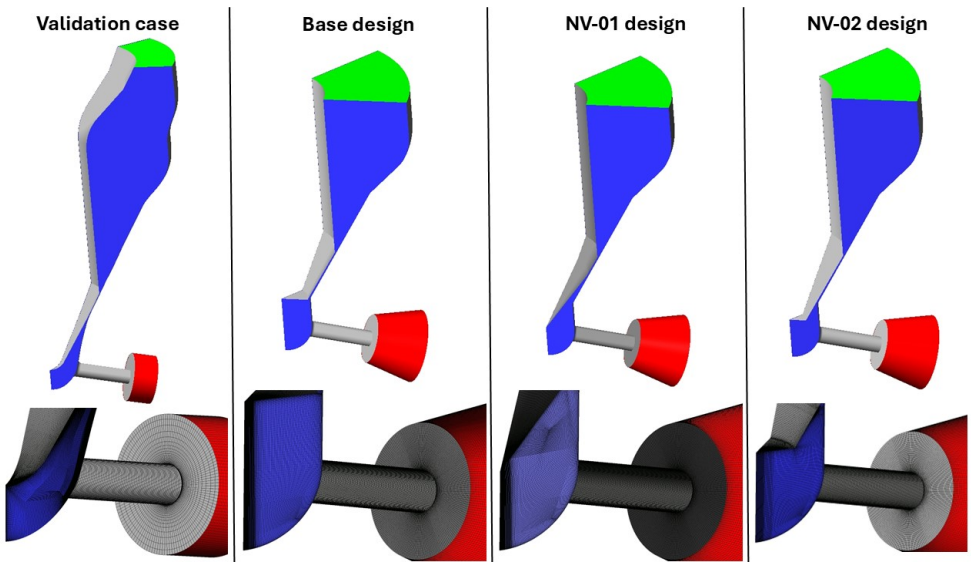

Figure 3.8: Geometries and computational domain.

3.1.2.3 Dynamic needle simulations

The computational domain used in this study consists of two distinct cell zones: the *sac region* and the *needle region*, as shown on the left side of Figure 3.9. The sac region remains stationary, while the needle region can either be fixed or move dynamically, depending on the simulation scenario. Two simulation cases are investigated in dynamic needle conditions:

- Lift only motion simulation: The needle follows a vertical lift profile (Figure 3.11).
- Wobbling motion simulation: The needle combines vertical lift with an off-axis displacement profile (Figure 3.11).

The computational grid, shown on the right side of Figure 3.9, includes 3.6 million cells in the *sac region* and 0.6 million cells in the *needle region*, resulting in a total of 4.2 million cells. The maximum y^+ value of 2 is localized near the needle seat entrance, while the typical y^+ value across the wall regions of the computational domain is lower, averaging around 1. This ensures sufficient wall resolution for the RANS $k-\omega$ SST turbulence model and aligns with best practices for this type of industrial simulation [68].

The inlet section of the sac is completely closed from the upstream position, which is a requirement for the overset methodology. The needle (red surface), as the moving component, is housed inside the stationary sac (dark grey surface), as shown on the left side of Figure 3.9. A total pressure of 2200 bar is applied at the inlet (green surface), representing a subsonic reservoir boundary condition. At the orifice outlet (blue surfaces), a static pressure of 10 bar is imposed. To reduce computational cost, additional downstream volumes beyond the orifice exit are not considered.

In the low lift position, the main focus is on the needle seat region, which refers to the area where the needle seals against the injector body to regulate the flow into the sac region, as shown in Figure 3.9. This region experiences the highest pressure drops and flow velocities, which promote cavitation and erosion. However, in (static) high lift cases, imposing boundaries directly at the orifice exit would significantly influence cavitation and erosion behaviors, as these phenomena occur entirely within the injector.

In the dynamic lift simulations, the overset mesh methodology is employed to manage the needle's motion. This approach uses an overset boundary, represented by the pink surface in the right side of the Figure 3.9, to facilitate

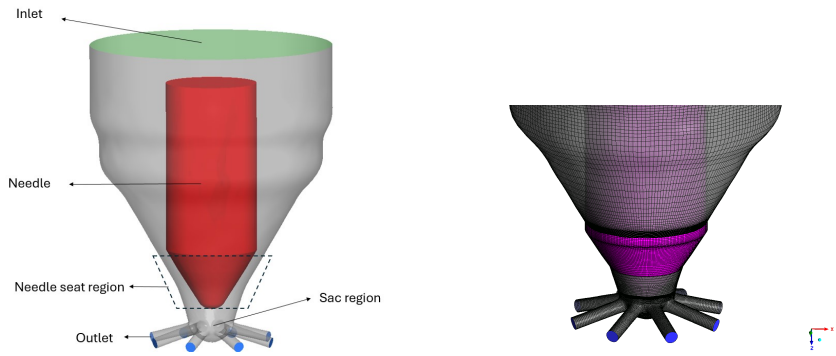

Figure 3.9: Model representation (left) and computational domain with the overset boundary (right).

seamless information exchange between the sac and needle regions. While this technique involves a comparatively high time cost for mesh and topology construction, it ensures superior grid quality for low needle positions and complex motions, such as wobbling motion. Unlike methods such as Cartesian cut-cell [36], node interpolation [20], or Arbitrary Lagrangian-Eulerian (ALE) methods [18], the overset approach avoids grid distortion, thereby improving overall accuracy.

The overset mesh methodology employs a dynamic "cutting and blanking" process that updates the overlapping grids in real time. This ensures accurate representation of the needle's motion while maintaining grid quality. Cut-plane representations of the overset grid at the lowest and highest lift positions are shown in Figure 3.10, demonstrating the capability of the mesh to accommodate complex needle dynamics. For static low lift simulation, the grid remains stationary, fixed at the 20 µm lift position.

The needle motion profiles (Figure 3.11) for the dynamic simulations are adapted from ECN Spray-A studies [36], with minor modifications to the off-axis profile to set the needle to its initial position. During the off-axis motion, the needle moves in both the negative y and x directions. This is visualized in Figure 3.12, with a red arrow showing the direction of the off-axis motion and the corresponding hole numbers. The needle ultimately moves towards the area between hole 2 and hole 3.

For all simulations, the computational grid is initialized with the needle

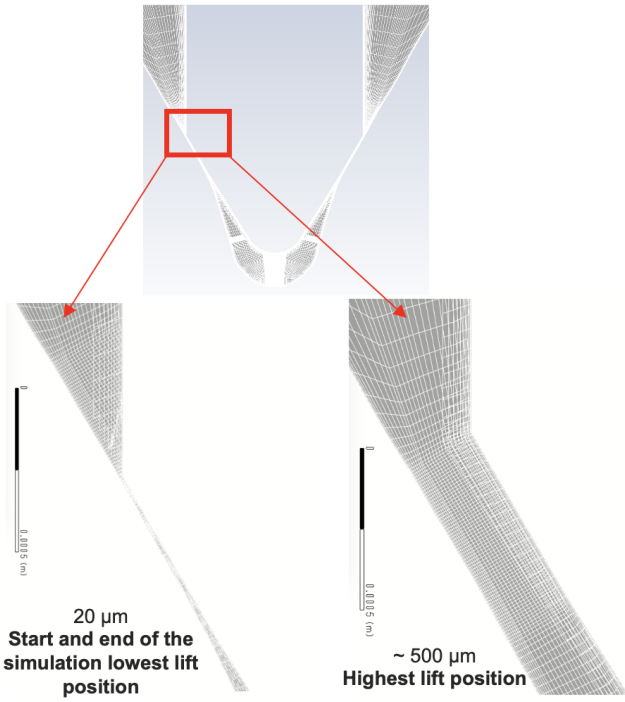

Figure 3.10: Cut-plane mesh representation of the overset mesh for the lowest (left) and highest (right) lift positions.

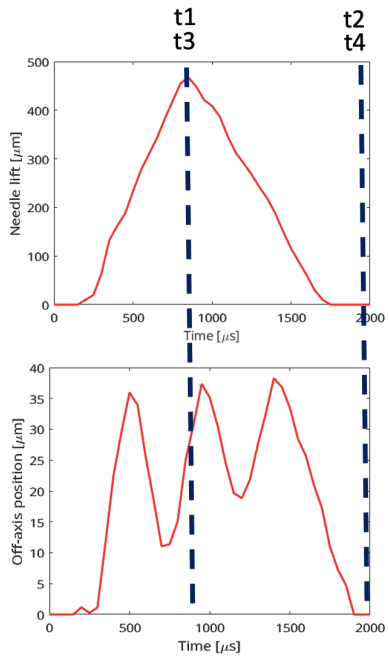

Figure 3.11: Lift (top) and off-axis (bottom) profiles with selected time instants (dashed lines) for erosion assessment.

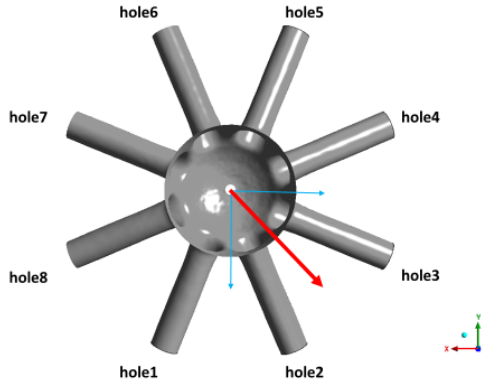

Figure 3.12: Direction of the off-axis motion.

fixed at a 20 µm lift position. This setup allows sufficient time for initial washout and transient flow effects to subside before collecting flow statistics and conducting erosion assessments.

3.2 Water-jet pump simulations

This work is described in more detail in Paper 4, where the related methodology and results are presented.

3.2.1 Operating conditions and experiment

The experiments were conducted in 2010 at the Kongsberg Hydrodynamic Research Centre (KHRC) in Kristinehamn, Sweden, using their free-surface cavitation tunnel. A soft paint erosion test was used to assess cavitation-induced damage on a mixed-flow pump. The tested impeller was a scaled-down prototype of a commercial water-jet pump, with a model inlet diameter of 200 mm. The impeller was coated with black stencil ink and thinner. Each test lasted one hour under controlled conditions. The removal of paint served as a qualitative indicator of cavitation erosion, identifying regions where cavitation

collapse was most aggressive [7].

Table 3.2 provides an overview of the operating conditions for each case. The tunnel water velocity (v_t) was recorded at a standard position 1400 mm upstream of the inlet lip using tunnel stationary equipment. The tunnel pressure (v_t) was measured in the air volume. The rotation rate was 20 rps for all cases.

The cavitation number (σ) is calculated using the tunnel pressure and tunnel water velocity, as expressed by the following equation:

$$\sigma = \frac{p_t - p_v}{\frac{1}{2}\rho v_t^2} \tag{3.2}$$

where, p_v is the vapor pressure of water (2065 [Pa]), and ρ is the water density (988.2 [kg/m^3]).

Studied case	**Tunnel velocity** v_t **[m/s]**	**Tunnel pressure** p_t **[Pa]**	**Flow rate** Q_e **[m^3/s]**	**Cavitation number,** σ
Case#1	4.85	18600	0.14400	1.410
Case#2	7.2	11800	0.15168	0.376
Case#3	8.7	17000	0.15648	0.395

Table 3.2: Summary of the operating conditions.

The cases were selected to investigate the distinct erosion patterns unique to each operating condition. This selection provides a robust way to evaluate the predictive capability of the numerical methodology by ensuring direct comparability between numerical predictions and experimentally observed erosion patterns. Figure 3.13 presents the erosion patterns observed at the end of the experiment for the selected cases. The top row displays the entire impeller, while the bottom row focuses on a single blade, highlighting the extent and distribution of cavitation-induced erosion.

The observations about experiments are summarized as follows:

- In Case#1, erosion was minimal, with only slight paint removal in the marked region.
- In Case#2, erosion was concentrated at the blade root. Weak pitting also developed in the mid-section of the blades.

- Case#3 had the most severe cavitation erosion. Extensive sheet erosion caused significant paint removal in the sheet region, while root erosion was similar to that in Case#2.

- There are signs of damage at the blade tips (marked in yellow), where painting is challenging. Hence, it is difficult to determine whether these marks result from cavitation erosion.

- Singular marks colored in blue are also present, which are not attributed to cavitation erosion but rather imperfections in the test procedure.

3.2.2 Geometry and computational domain

Figure 3.14 illustrates the main topology of the computational domain. The flow enters through a rectangular inlet channel and splits into two primary streams. One stream flows into the rotor region through a flush-type intake duct, while the remaining flow continues toward the tunnel outlet.

The inlet is defined as a velocity inlet, while the pump and tunnel outlets are set as pressure outlets. To ensure consistency with the experimental setup, the inlet velocity values in the simulations match the tunnel velocities measured approximately 1400 mm upstream of the inlet lip. Table 3.3 presents the velocity and pressure values used in the simulations, corresponding to the experimental operating conditions in Table 3.2.

Despite relatively shallow depth of the tunnel outlet's, hydrostatic effects are incorporated by implementing a hydrostatic boundary condition at the outlet. The reference location for hydrostatic pressure is defined at the rotor axis. This boundary condition had a noticeable impact on the results, as using the hydrostatic pressure profile instead of a constant tunnel pressure value led to a decrease in total vapor volume within the rotor region.

The back pressure on the pump outlet influences the cavitation dynamics and cavitation erosion behavior by affecting the pressure distribution and vapor collapse characteristics. In this study, the air is included primarily to provide realistic tunnel pressure (which was measured with air volume) conditions in the experiment.

A no-slip boundary condition is applied to the pump casing, hub, stator, duct, and upper tunnel walls. The tunnel's side and bottom surfaces are set as

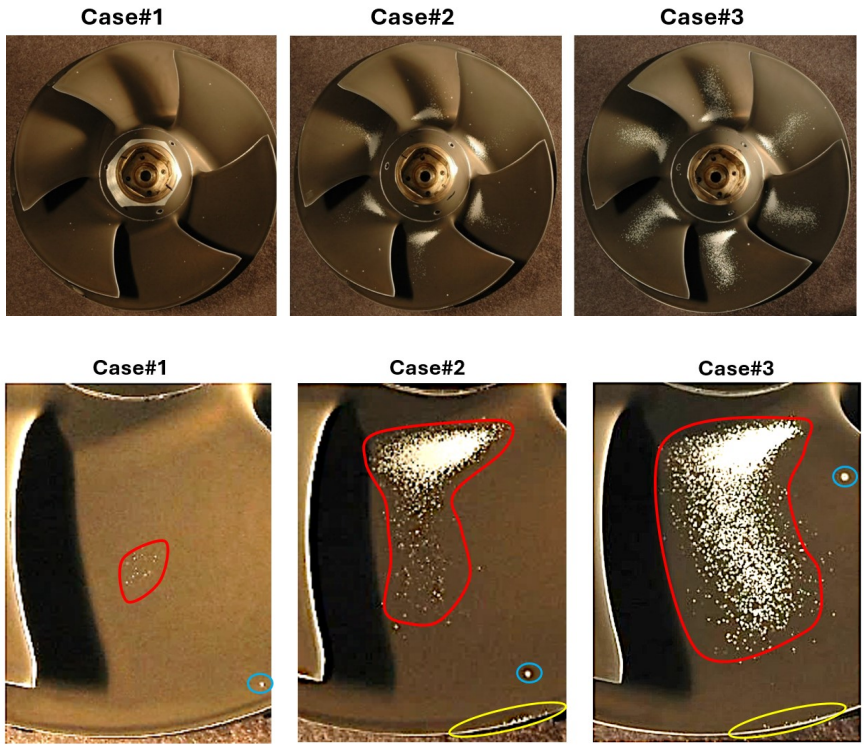

Figure 3.13: Erosion patterns for the selected cases. Top row: full impeller view; Bottom row: single blade close-up.

Table 3.3: Boundary conditions.

Studied case	Inlet Velocity (m/s)	Outlet Pressure (Pa)
Case#1	3.725	18600
Case#2	5.529	11800
Case#3	6.681	17000

slip boundaries. Rotating and stationary regions interact through predefined interfaces.

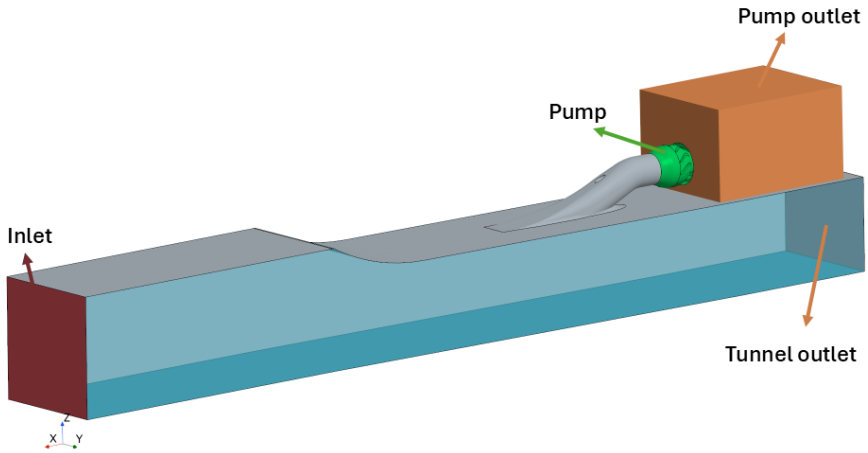

Figure 3.14: Geometry and boundary conditions.

Besides the aforementioned cavitation erosion assessment using the maximum $(DP/Dt)^2$ values on the surfaces, the pitting behavior on the rotor blades is additionally investigated. In this analysis, one blade is selected and divided into two distinct regions: the sheet region and the root region, as transparently illustrated in Figure 3.15. The sheet region, highlighted in green, represents the larger portion of the blade, while the root region, shown in red, corresponds to the section near the hub. The force acting on these surfaces was integrated separately for each case to assess the localized effects of flow and cavitation dynamics.

To facilitate a meaningful comparison between different regions, the total force acting on each region was normalized by the corresponding surface area.

Figure 3.15: Representation of the root and sheet region on selected blade.

This normalization ensures that the force values are independent of the size of each region, allowing for a *pressure-like* interpretation. The normalized force per unit area, denoted as $\bar{F}$, is computed as:

$$\bar{F} = \frac{F_{\text{region}}}{A_{\text{region}}} \tag{3.3}$$

where F_{region} represents the integrated force acting on either the *sheet* or *root* region, and A_{region} denotes the corresponding surface area.

To assess the effect of grid resolution on numerical simulations, three computational grids were generated and tested with Case#3 condition. These grids, labeled as Baseline, Coarse, and Refined, differ in spatial resolution and total cell count. Table 3.4 summarizes the number of cells in different regions of the computational domain.

In the coarse grid, the base size was set to 1/50 of the rotor diameter (0.27 m), resulting in 5.4 mm. The baseline grid further halved the base cell size, achieving a 2.7 mm grid resolution. The Refined grid was obtained by further refining only the rotating region while keeping the inlet and outlet channels identical to the Baseline configuration.

Figure 3.16 presents the impeller surface mesh of the Baseline grid. The inlet channel primarily utilizes hexahedral cells, generated using a trimmed cell mesher. Meanwhile, the rotating impeller region and outlet channel are meshed using polyhedral cells, allowing for better adaptability to complex geometries and improved numerical stability.

Table 3.4: Number of cells for different regions of the computational domain for different grid configurations.

Region	**Coarse**	**Baseline**	**Refined**
Inlet channel	4.0×10^6	15.7×10^6	15.7×10^6
Outlet channel	1.3×10^6	4.1×10^6	4.1×10^6
Rotating region	2.7×10^6	7.0×10^6	19.4×10^6
Total Cells	8.0×10^6	26.8×10^6	39.2×10^6

Table 3.5 presents the total vapor volume and vapor flow rate for different grid resolutions. Despite varying grid refinement levels, the total vapor volume and volume flow rates remain nearly identical, indicating consistent numerical predictions across different mesh configurations. The flow rate pre-

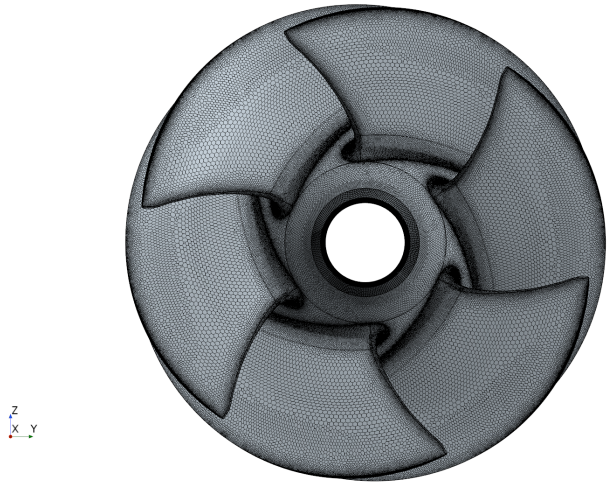

Figure 3.16: Surface mesh representation of the impeller.

dictions obtained from the numerical simulations are also compared with the experimental flow rate of 0.15648 m^3/s. The results showed that each grid shows around 1-2 % deviation from the experimental flow rate. Despite the finer grid resolution, the improvement in flow rate prediction remained limited, indicating that all grids capture the systematic flow properties with sufficient accuracy.

To further evaluate the effect of grid resolution on cavitation erosion predictions, a comparative analysis was conducted across all grid configurations. Figure 3.17 presents the maximum values of the $(DP/Dt)^2$ for the coarse, baseline, and refined grids. The refined grid captures wider erosion patterns over the sheet region. In contrast, the coarse grid failed to capture the root erosion observed in the experiment (see Figure 3.13, Case#3). Thus, the refined grid aligns more closely with the experimental observations.

While further grid refinement is theoretically possible, as demonstrated in LES studies by Arabnejad et al. [5], [63], achieving LES-level accuracy requires significantly higher resolutions. These studies emphasize the need for higher grid resolutions to resolve the turbulent structures accurately. In particular, they highlight that at least 40 cells inside the tip gap are necessary to successfully capture the Tip Leakage Vortex (TLV) phenomena. However,

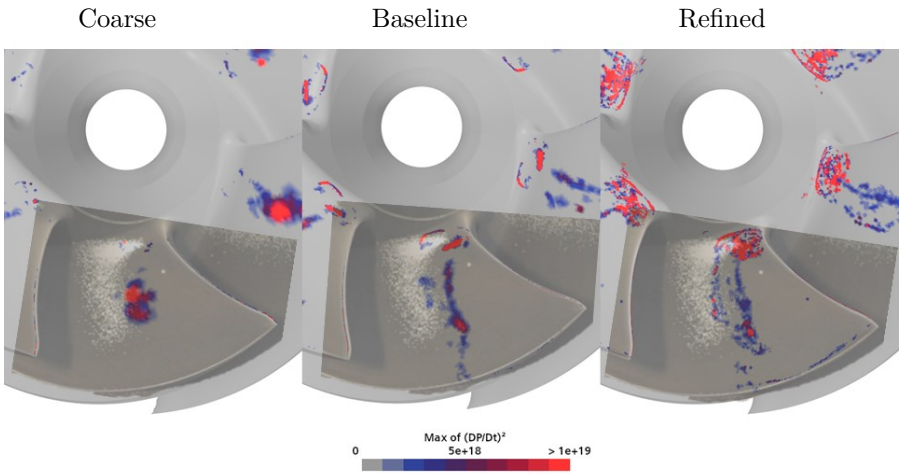

Figure 3.17: Comparison of maximum $(DP/Dt)^2$ values for cavitation erosion prediction using different grid resolutions. The experimental images are overlaid transparently for direct visual correlation.

this study aims to provide a reliable erosion assessment tool while ensuring computational efficiency. The use of RANS-based modeling makes it a viable approach for industrial applications. It is clear from the Figure 3.17 that although the refined grid captures more detailed erosion zones, the baseline grid provides sufficient accuracy with an acceptable resolution. Therefore, considering the overall computational cost of all simulations, all subsequent simulations will be conducted using the baseline grid.

Table 3.5: Comparison of total vapor volume and volume flow rate for each grid configurations.

Grid	**Total vapor volume (mm^3)**	**Volume flow rate (m^3/s)**
Coarse	4456	0.1546
Baseline	4375	0.1547
Refined	4252	0.1545

CHAPTER 4

Summary of the Appended Papers

This chapter presents a summary of the appended papers. Each section discusses the aim and main conclusions of the individual studies.

4.1 Paper 1

Mehmet Özgünoğlu, Gerard Mouokue, Michael Oevermann, Rickard E. Bensow, *Numerical investigation of cavitation erosion in high-pressure fuel injectors in the presence of surface deviations*, Fuel, vol. 386 (2025), pp. 134174. doi:10.1016/j.fuel.2024.134174.

4.1.1 Contribution

The author of this thesis contributed to the planning and writing of the paper, developed the numerical model for assessing cavitation erosion in high-pressure fuel injectors, performed the simulations and post-processing of the numerical results, and contributed to the interpretation of the findings.

4.1.2 Aim

This study examines the impact of surface deviations on cavitation erosion in high-pressure fuel injector under static high lift condition. The research employs both RANS and LES simulations using CAD and TS geometries to assess the effects of idealized versus realistic geometries. Additionally, a comprehensive evaluation of erosion indicators is conducted to determine the most suitable metric for predicting cavitation erosion risk. Furthermore, both 1-hole and 8-hole simulations are performed to investigate the variability of cavitation erosion across different injector orifices.

4.1.3 Results and Conclusion

The study finds that surface deviations significantly modify cavitation erosion patterns by reducing vapor volumes and altering collapse locations. The TS model, which includes real-world deviations, provides better agreement with experimental erosion data than the CAD model. Among the different erosion indicators tested, the squared material derivative of pressure $(DP/Dt)^2$ is identified as the most reliable predictor of erosion-prone regions.

The 8-hole simulations reveal that each orifice exhibits distinct cavitation and erosion behaviors, emphasizing the need for localized assessments rather than relying on single-hole simulations alone. Differences in surface deviations among the holes lead to variations in erosion intensity and distribution, further validating the necessity of incorporating realistic manufacturing variations in numerical models.

LES simulations offer greater detail in capturing cavitation structures and turbulence interactions compared to RANS, but at a computational cost nearly 32 times higher. Despite its lower computational expense, RANS-based predictions still align well with experimental observations, making it a practical choice for large-scale injector assessments.

The study concludes that incorporating realistic surface deviations and multi-hole analyses into numerical simulations is crucial for improving erosion risk assessments in fuel injection systems. These findings provide valuable insights for optimizing injector designs and refining predictive models for cavitation erosion.

4.2 Paper 2

Mehmet Özgünoğlu, Gerard Mouokue, Michael Oevermann, Rickard E. Bensow, *Numerical study of cavitation erosion in high-pressure fuel injectors: The role of wobbling motion*, Under review in Wear.

4.2.1 Contribution

The author of this thesis contributed to the planning and writing of the paper, implemented the numerical framework for modeling injector needle motion effects, conducted the cavitation erosion risk assessment and validation against experimental observations.

4.2.2 Aim

This study explores the role of transient needle motion, particularly wobbling motion, in influencing cavitation formation and erosion risk in high-pressure fuel injectors. Wobbling motion refers to lateral off-axis displacement of the needle, which occurs due to manufacturing tolerances and fluid-induced forces. The objective is to determine how this motion affects cavitation erosion.

4.2.3 Results and Conclusion

The results demonstrate that wobbling motion redistributes pressure loads associated with cavitation collapses, reducing localized erosion severity compared to purely vertical lift motion. Static low lift simulations reveal erosion-prone regions near the needle tip and upstream of the orifice inlet, aligning well with experimental data.

Dynamic simulations show that wobbling motion alters the intensity and distribution of pressure pulses on injector surfaces, leading to a more dispersed erosion pattern. The study suggests that while wobbling motion is not intentionally controlled, it has a noticeable effect on cavitation-induced erosion, providing valuable insights for injector design. These findings highlight the importance of incorporating transient needle dynamics into numerical erosion assessments.

4.3 Paper 3

Mehmet Özgünoğlu, Marilia G. J. Vaz, Michael Oevermann, Rickard E. Bensow, Manolis Gavaises, Gerard Mouokue, *Effect of thermodynamic modeling and design variations on cavitation erosion in high-pressure fuel injectors*, Manuscript.

4.3.1 Contribution

The author of this thesis contributed to the planning of the study, conducted all numerical simulations, applied cavitation erosion modeling to all cases, and created the computational mesh for the validation case. Additionally, the author contributed to the interpretation of results related to cavitation erosion and its dependence on design variations.

4.3.2 Aim

This study investigates the role of thermodynamic modeling and design variations in predicting cavitation erosion in high-pressure fuel injectors. The goal is to assess how different modeling approaches affect cavitation behavior and erosion risk.

4.3.3 Results and conclusion

This study examined the impact of thermodynamic modeling and needle design variations on cavitation erosion in high-pressure fuel injectors. The PC-SAFT&CV model, incorporating compressible vapor and temperature-dependent phase transitions, provided more realistic predictions of vapor structures and erosion localization compared to the Tait&IV approach.

Cavitation erosion risk was then examined for three needle designs. The base design generated the highest vapor content, but erosion remained relatively moderate. NV-01, featuring a divergent tip, reduced vapor volume but exhibited intensified erosion near the sac due to unstable vapor collapses. NV-02, with an elongated needle tip, provided a more balanced erosion profile by confining collapse activity, though some localized damage persisted.

Across all cases, cavitation erosion was assessed using the squared material derivative of pressure, $(DP/Dt)^2$, which was a reliable indicator of high-intensity collapse zones. Comparison with experimental data confirmed that

the PC-SAFT&CV model predicted sac- and needle-side erosion locations with greater accuracy. The results highlight that design-induced changes in collapse behavior and associated thermal gradients play a critical role in long-term injector durability. Geometrical modifications in the needle altered cavitation inception and collapse dynamics, emphasizing the importance of design optimization in minimizing erosion and associated thermal stresses.

4.4 Paper 4

Mehmet Özgünoğlu, Martin Persson, Ammar Saber, Rickard E. Bensow, *Numerical prediction of cavitation erosion in a water-jet propulsion system*, Under review in Ocean Engineering.

4.4.1 Contribution

The author of this thesis contributed to the planning and writing of the paper, developed and implemented the numerical model for water-jet pump cavitation, performed the simulations and analyzed cavitation-induced pressure loads to assess erosion risk.

4.4.2 Aim

This study presents a numerical cavitation erosion assessment for a water-jet pump using a RANS-based framework with the Schnerr-Sauer cavitation model. The erosion risk is evaluated using the squared material derivative of pressure $(DP/Dt)^2$. Three different operating conditions are analyzed to assess the impact of inlet velocity and pressure on cavitation behavior. The numerical results are validated against experimental soft paint erosion tests conducted at KHRC.

4.4.3 Results and Conclusion

The study shows that operating conditions significantly influence cavitation behavior. Higher inlet velocities lead to increased asymmetry in velocity and pressure fields, affecting cavitation structures and erosion distribution. The erosion risk metric $(DP/Dt)^2$ successfully identifies erosion-prone regions, particularly in the sheet and root areas of the impeller blades.

However, the numerical model underestimates the extent of erosion, especially in Case#2 and Case#3, due to the deterministic nature of RANS simulations. The inability to resolve transient cavitation structures, re-entrant jets, and small-scale collapses limits accuracy in predicting erosion severity. The normalized force analysis highlights strong pressure fluctuations in Case#2 and Case#3, aligning with observed erosion patterns.

Despite these limitations, the RANS-based approach provides a computationally efficient tool for early-stage cavitation erosion assessment in industrial applications. Future improvements should focus on hybrid RANS-LES modeling and enhanced erosion prediction techniques.

CHAPTER 5

Concluding Remarks

5.1 Summary

This dissertation presents a numerical investigation of cavitation erosion phenomena in high-pressure fuel injectors and water-jet propulsion systems. The research employs Computational Fluid Dynamics (CFD) methodologies, focusing on turbulence modeling, cavitation closure models, and erosion prediction techniques. The findings contribute to the development of predictive erosion assessment frameworks applicable to industrial applications.

For high-pressure fuel injectors, the research examines both static and dynamic lift conditions, emphasizing the role of surface deviations and transient needle motion. The static high lift study demonstrates that surface deviations significantly influence cavitation erosion by modifying vapor collapse locations and intensities. The 8-hole simulations reveal variations in cavitation structures across different orifices, highlighting the importance of multi-hole analyses for accurate erosion predictions. Additionally, a comparative study of erosion indicators confirms that the squared material derivative of pressure, $(DP/Dt)^2$, provides the most reliable assessment of cavitation erosion risk.

The study of transient needle motion focuses on wobbling effects, showing

that off-axis displacement redistributes cavitation-induced pressure loads, reducing localized erosion patterns. While wobbling motion cannot be directly controlled, its influence on erosion risk suggests potential implications for injector design and operational strategies.

The final study on the fuel injectors examines the influence of thermodynamic modeling and needle design variations on cavitation erosion prediction. The Perturbed-Chain Statistical Associating Fluid Theory with Compressible Vapor (PC-SAFT&CV) model, which accounts for vapor compressibility and temperature-dependent thermodynamic behavior, was found to predict vapor collapse dynamics and erosion localization more accurately than the Tait equation of state with Incompressible Vapor (Tait&IV) model. Moreover, simulations with different needle tip geometries revealed that small design changes can significantly affect vapor distribution and collapse behavior, thereby influencing erosion severity. These findings underscore the importance of combining thermodynamic fidelity with targeted geometric optimization for improved erosion prediction.

In the water-jet propulsion study, a RANS-based erosion risk assessment framework is developed using the Schnerr-Sauer cavitation model and $(DP/Dt)^2$. The results demonstrate that operating conditions strongly influence cavitation behavior, with variations in inlet velocity and pressure affecting the extent and distribution of vapor collapses. While numerical predictions correctly capture high-risk cavitation collapse regions, the RANS-based approach underestimates erosion extent due to its limitations in resolving transient cavitation structures. The study identifies peak force fluctuations corresponding to major collapse events, reinforcing the correlation between cavitation dynamics and erosion risk.

- Development and validation of a numerical cavitation erosion assessment methodology applicable to both fuel injectors and water-jet pumps.
- Investigation of transient needle motion effects, particularly wobbling, on cavitation erosion patterns.
- Demonstration of the significance of surface deviations in cavitation-induced erosion, emphasizing the need for realistic geometry modeling and multi-hole simulations.
- Evaluation of thermodynamic modeling approaches, highlighting the importance of compressible, temperature-dependent vapor modeling for

accurate erosion prediction.

- Assessment of needle design variations, showing that subtle geometric differences significantly influence vapor collapse and erosion risk.
- Implementation of a computationally efficient RANS-based erosion risk assessment tool for industrial applications.
- Analysis of cavitation behavior under different operating conditions in water-jet propulsion, linking force fluctuations to erosion severity.

These contributions directly fulfill the objectives outlined in Section 1.3. The proposed CFD erosion assessment methodology achieves the intended balance between accuracy and computational efficiency, making it applicable within industrial time frames. The investigations into turbulence and thermodynamic modeling, surface deviations, and needle dynamics explicitly address the influence of modeling and design parameters on erosion prediction. Additionally, the validation of erosion risk indicators—especially $(DP/Dt)^2$—across different configurations supports the objective of identifying robust predictive metrics. By covering both fuel injector and water-jet pump cases, the thesis ensures broad applicability of the proposed framework across different fluid machinery types.

5.2 Future Work

While this research provides valuable insights into cavitation erosion mechanisms, several areas merit further investigation and development:

1. **Enhanced LES simulations for fuel injectors**
   Future work should apply LES to full 8-hole diesel injector configurations under both high and low needle lift conditions. These simulations can resolve asymmetric cavitation behavior and hole-to-hole interaction effects that RANS fails to capture. LES data can also serve as a reference to calibrate simplified models for industrial use, helping to bridge the gap between physical fidelity and computational feasibility.
2. **Advanced needle dynamics modeling**
   The start-up and closure phases of needle motion—where rapid transients dominate—remain largely unexplored but may play a critical role

in early-stage erosion formation. Simulations should examine the effect of needle acceleration and deceleration on vapor collapse near the seat and sac, particularly in off-axis scenarios.

3. **Refinement of erosion risk metrics**
   While $(DP/Dt)^2$ has shown strong correlation with erosion-prone zones, future studies could explore cumulative energy-based metrics, such as time-integrated pressure impulses or collapse impulse frequency. These should be evaluated against long-duration experimental erosion patterns (e.g., soft paint or epoxy tests) and tested for sensitivity across geometries and operating conditions. Another promising direction is combining local stress prediction with collapse localization to estimate material response more directly.

4. **Hybrid RANS-LES modeling for water-jet propulsion**
   To maintain industrial time scale viability, hybrid approaches like DDES (Delayed Detached Eddy Simulation) or WMLES (Wall-Modeled LES) can be applied to water-jet pump cases. These methods may better capture unsteady cavity shedding and collapse phenomena without the prohibitive cost of full LES.

5. **Exploration of cavitation mitigation strategies**
   Needle tip geometry modifications—such as controlled chamfering or asymmetrical inlet rounding—could be systematically evaluated for their ability to reduce collapse intensity. Combined with dynamic simulations, studies could also explore partial-lift injection schedules or multi-pulse strategies to modulate cavitation risk over the injection cycle. These investigations would inform practical design guidelines to mitigate erosion without sacrificing performance.

6. **Broadening the scope of water-jet pump applications**
   The current framework could be extended to analyze erosion in mixed-flow or radial-flow pump geometries. Future work should evaluate the impact of blade angle variation, hub-tip ratio, and casing treatments on cavitation behavior across multiple operating regimes. Parameter sweeps could identify design thresholds that either suppress or amplify cavitation collapse risks.

Addressing these areas will help advance predictive cavitation erosion modeling while preserving computational feasibility. The long-term goal is to deliver practical tools that support robust design optimization under real-world constraints.

References

[1] J.-P. Franc and J.-M. Michel, *Fundamentals of Cavitation* (Fluid Mechanics and Its Applications). Springer Dordrecht, 2004, vol. 76, ISBN: 978-1-4020-2232-6.

[2] S. J. Schmidt, M. S. Mihatsch, M. Thalhamer, and N. A. Adams, "Assessment of erosion sensitive areas via compressible simulation of unsteady cavitating flows," *Fluid Mechanics and its Applications*, K.-H. Kim, G. Chahine, J.-P. Franc, and A. Karimi, Eds., pp. 329–344, 2014.

[3] W.-G. Park, J. H. Jang, H. H. Chun, and M. C. Kim, "Numerical flow and performance analysis of waterjet propulsion system," *Ocean Engineering*, vol. 32, no. 14, pp. 1740–1761, 2005, ISSN: 0029-8018.

[4] G. Bark, N. Berchiche, and M. Grekula, "Application of principles for observation and analysis of eroding cavitation-the erocav observation handbook," *EROCAV Report, Dept. of Naval Architecture, Chalmers University of Technology, Göteborg, Sweden*, 2004.

[5] M. H. Arabnejad, U. Svennberg, and R. E. Bensow, "Numerical assessment of cavitation erosion risk in a commercial water-jet pump," *Journal of Fluids Engineering*, vol. 144, no. 5, p. 051 201, Jan. 2022, ISSN: 0098-2202.

[6] B. Aktas, O. Usta, and M. Atlar, "Systematic investigation of coating application methods and soft paint types to detect cavitation erosion on marine propellers," *Applied Ocean Research*, vol. 94, p. 101 868, 2020.

[7] F. Alves Pereira, R. Boucheron, D. Boucetta, C. Fetherstonhaugh, P. Krol, Y. Pang, C. Park, K. Sato, W. A. Straka, and V. Viitanen, "Cavitation induced erosion on propellers and rudders, model scale experiments and numerical guidance," International Towing Tank Conference (ITTC), Switzerland, Tech. Rep. 7.5-02-03-03.5, May 2024, ITTC Recommended Procedures and Guidelines, Revision 03.

[8] M. Dular, B. Stoffel, and B. Širok, "Development of a cavitation erosion model," *Wear*, vol. 261, no. 5, pp. 642–655, 2006, ISSN: 0043-1648.

[9] M. Dular and O. Coutier-Delgosha, "Numerical modelling of cavitation erosion," *International Journal for Numerical Methods in Fluids*, vol. 61, no. 12, pp. 1388–1410, 2009.

[10] R. E. Bensow and G. Bark, "Implicit LES Predictions of the Cavitating Flow on a Propeller," *Journal of Fluids Engineering*, vol. 132, no. 4, p. 041 302, Apr. 2010, ISSN: 0098-2202.

[11] Z.-r. Li, M. Pourquie, and T. van Terwisga, "Assessment of Cavitation Erosion With a URANS Method," *Journal of Fluids Engineering*, vol. 136, no. 4, p. 041 101, Feb. 2014, ISSN: 0098-2202.

[12] M. S. Mihatsch, S. J. Schmidt, and N. A. Adams, "Cavitation erosion prediction based on analysis of flow dynamics and impact load spectra," *Physics of Fluids*, vol. 27, no. 10, p. 103 302, Oct. 2015, ISSN: 1070-6631.

[13] A. Peters, H. Sagar, U. Lantermann, and O. el Moctar, "Numerical modelling and prediction of cavitation erosion," *Wear*, vol. 338-339, pp. 189–201, 2015, ISSN: 0043-1648.

[14] A. Peters and O. el Moctar, "Numerical assessment of cavitation-induced erosion using a multi-scale euler–lagrange method," *Journal of Fluid Mechanics*, vol. 894, A19, 2020.

[15] S. Schenke and T. van Terwisga, "An energy conservative method to predict the erosive aggressiveness of collapsing cavitating structures and cavitating flows from numerical simulations," *International Journal of Multiphase Flow*, vol. 111, pp. 200–218, 2019, ISSN: 0301-9322.

[16] M. H. Arabnejad, U. Svennberg, and R. E. Bensow, "Numerical assessment of cavitation erosion risk using incompressible simulation of cavitating flows," *Wear*, vol. 464-465, p. 203 529, 2021, ISSN: 0043-1648.

[17] F. Örley, S. Hickel, S. J. Schmidt, and N. A. Adams, "Large-eddy simulation of turbulent, cavitating fuel flow inside a 9-hole diesel injector including needle movement," *International Journal of Engine Research*, vol. 18, no. 3, pp. 195–211, 2017.

[18] K. Kolovos, N. Kyriazis, P. Koukouvinis, A. Vidal, M. Gavaises, and R. M. McDavid, "Simulation of transient effects in a fuel injector nozzle using real-fluid thermodynamic closure," *Applications in Energy and Combustion Science*, vol. 7, p. 100 037, 2021, ISSN: 2666-352X.

[19] S. Falsafi, M. Blume, T. Klaua, M. Indrich, J. Wloka, and R. Skoda, "Numerical simulation of cavitating flow in maritime high-pressure direct fuel injection nozzles and assessment of cavitation-erosion damage," *International Journal of Engine Research*, vol. 24, no. 2, pp. 393–407, 2023.

[20] E. Gomez Santos, J. Shi, R. Venkatasubramanian, G. Hoffmann, M. Gavaises, and W. Bauer, "Modelling and prediction of cavitation erosion in GDi injectors operated with e100 fuel," *Fuel*, vol. 289, p. 119 923, 2021, ISSN: 0016-2361.

[21] P. Koukouvinis, M. Gavaises, J. Li, and L. Wang, "Large eddy simulation of diesel injector including cavitation effects and correlation to erosion damage," *Fuel*, vol. 175, pp. 26–39, 2016, ISSN: 0016-2361.

[22] P. Koukouvinis, I. K. Karathanassis, and M. Gavaises, "Prediction of cavitation and induced erosion inside a high-pressure fuel pump," *International Journal of Engine Research*, vol. 19, no. 3, pp. 360–373, 2018.

[23] M. Brunhart, "Cavitation and the application of methods for erosion prediction in high pressure fuel injection systems," Ph.D. dissertation, City, University of London, 2020.

[24] R. Fortes Patella, A. Archer, and C. Flageul, "Numerical and experimental investigations on cavitation erosion," *IOP Conference Series: Earth and Environmental Science*, vol. 15, pp. 2013–, Nov. 2012.

[25] M. Cristofaro, W. Edelbauer, P. Koukouvinis, and M. Gavaises, "Large Eddy Simulation of the Internal Injector Flow During Pilot Injection," in *Proceedings of the 10th International Symposium on Cavitation (CAV2018)*, ASME Press, Dec. 2018, ISBN: 9780791861851.

[26] M. Cristofaro, W. Edelbauer, P. Koukouvinis, and M. Gavaises, "A numerical study on the effect of cavitation erosion in a diesel injector," *Applied Mathematical Modelling*, vol. 78, pp. 200–216, 2020, ISSN: 0307-904X.

[27] M. Cristofaro, W. Edelbauer, P. Koukouvinis, and M. Gavaises, "Influence of diesel fuel viscosity on cavitating throttle flow simulations under erosive operation conditions," *ACS Omega*, vol. 5, no. 13, pp. 7182–7192, 2020, PMID: 32280858.

[28] A. V. Morozov, U. Iben, and R. Bosch, "Experimental analysis and simulation of cavitating throttle flow," 2008.

[29] L. Zhang, Z. He, W. Guan, Q. Wang, and S. Som, "Simulations on the cavitating flow and corresponding risk of erosion in diesel injector nozzles with double array holes," *International Journal of Heat and Mass Transfer*, vol. 124, pp. 900–911, 2018, ISSN: 0017-9310.

[30] A. Kumar, A. Ghobadian, and J. Nouri, "Numerical simulation and experimental validation of cavitating flow in a multi-hole diesel fuel injector," *International Journal of Engine Research*, vol. 23, no. 6, pp. 958–973, 2022.

[31] C. Wang, M. Adams, T. Luo, T. Jin, F. Luo, and M. Gavaises, "Hole-to-hole variations in coupled flow and spray simulation of a double-layer multi-holes diesel nozzle," *International Journal of Engine Research*, vol. 22, no. 10, pp. 3233–3246, 2021.

[32] G. M. Magnotti, M. Battistoni, K. Saha, and S. Som, "Development and validation of the cavitation-induced erosion risk assessment tool," *Transportation Engineering*, vol. 2, p. 100 034, 2020, ISSN: 2666-691X.

[33] F. Mariasiu, "Numerical investigation of the effects of biofuel characteristics on the injector nozzle erosion process," *Tribology Transactions*, vol. 56, no. 2, pp. 161–168, 2013.

[34] S. Mouvanal, D. Chatterjee, S. Bakshi, A. Burkhardt, and V. Mohr, "Numerical prediction of potential cavitation erosion in fuel injectors," *International Journal of Multiphase Flow*, vol. 104, pp. 113–124, 2018, ISSN: 0301-9322.

[35] Greif, David and Srinivasan, Vedanth, "Numerical prediction of erosive cavitating flows in injection equipment," in *10th International Conference on Engines and Vehicles*, SAE International, Sep. 2011.

[36] Q. Xue, S. Som, M. Battistoni, D. Longman, H. Zhao, P. Senecal, and E. Pomraning, "Three-dimensional simulations of the transient internal flow in a diesel injector: Effects of needle movement," May 2013.

[37] B. M Devassy, D. Greif, and W. Edelbauer, "Study of cavitation and 3d needle movement due to erosion in fuel injection nozzles using coupled simulation tools," in *Proceedings of the 18th Annual Conference on Liquid Atomization and Spray Systems (ILASS-Asia)*, Nov. 2016.

[38] H. Zhao, S. Quan, M. Dai, E. Pomraning, P. K. Senecal, Q. Xue, M. Battistoni, and S. Som, "Validation of a three-dimensional internal nozzle flow model including automatic mesh generation and cavitation effects," *Journal of Engineering for Gas Turbines and Power*, vol. 136, no. 9, p. 092 603, Apr. 2014, ISSN: 0742-4795.

[39] M. Battistoni, Q. Xue, S. Som, and E. Pomraning, "Effect of off-axis needle motion on internal nozzle and near exit flow in a multi-hole diesel injector," *SAE International Journal of Fuels and Lubricants*, vol. 7, no. 1, pp. 167–182, 2014, ISSN: 19463952, 19463960.

[40] N. Papadopoulos and P. Aleiferis, "Numerical modelling of the in-nozzle flow of a diesel injector with moving needle during and after the end of a full injection event," *SAE International Journal of Engines*, vol. 8, no. 5, pp. 2285–2302, 2015, ISSN: 19463936, 19463944.

[41] D. Greif, P. Sampl, and W. Edelbauer, "Cavitating injector flow simulations considering longitudinal and lateral needle displacement," *International Journal of Automotive Engineering*, vol. 5, no. 2, pp. 85–90, 2014.

[42] G. Guo, Z. He, Q. Wang, M.-C. Lai, W. Zhong, W. Guan, and J. Wang, "Numerical investigation of transient hole-to-hole variation in cavitation regimes inside a multi-hole diesel nozzle," *Fuel*, vol. 287, p. 119 457, 2021, ISSN: 0016-2361.

[43] T. Melissaris, N. Bulten, and T. van Terwisga, "On the applicability of cavitation erosion risk models with a urans solver," *Journal of Fluids Engineering*, vol. 141, no. 10, p. 101 104, Apr. 2019, ISSN: 0098-2202.

[44] T. Melissaris, S. Schenke, N. Bulten, and T. van Terwisga, "On the accuracy of predicting cavitation impact loads on marine propellers," *Wear*, vol. 456-457, p. 203 393, 2020, ISSN: 0043-1648.

[45] T. Melissaris, S. Schenke, N. Bulten, and T. van Terwisga, "Cavitation erosion risk assessment on a full-scale steerable thruster," *Ocean Engineering*, vol. 251, p. 111 019, 2022.

[46] R. Huang, Y. Wang, T. Du, X. Luo, W. Zhang, and Y. Dai, "Mechanism analyses of the unsteady vortical cavitation behaviors for a waterjet pump in a non-uniform inflow," *Ocean Engineering*, vol. 233, p. 108 798, 2021, ISSN: 0029-8018.

[47] R. E. Bensow, "Chapter 4 - numerical prediction of cavitation and related nuisances in marine propulsion systems," in *Cavitation and Bubble Dynamics*, P. Koukouvinis and M. Gavaises, Eds., Academic Press, 2021, pp. 111–132, ISBN: 978-0-12-823388-7.

[48] O. Usta, B. Aktas, M. Maasch, O. Turan, M. Atlar, and E. Korkut, "A study on the numerical prediction of cavitation erosion for propellers," *Proceedings of the Fifth International Symposium on Marine Propulsion*, 2017.

[49] O. Usta and E. Korkut, "A study for cavitating flow analysis using des model," *Ocean Engineering*, vol. 160, pp. 397–411, 2018.

[50] C. S. Koksal, O. Usta, B. Aktas, M. Atlar, and E. Korkut, "Numerical prediction of cavitation erosion to investigate the effect of wake on marine propellers," *Ocean Engineering*, vol. 239, p. 109 820, 2021.

[51] K. W. Shin and P. Andersen, "Practical numerical method for erosion risk prediction on ship propellers," *International Shipbuilding Progress*, vol. 67, pp. 199–220, 2020.

[52] M. Wheeler, A. Peters, O. el Moctar, M. Persson, A. Gunderson, D. Frisk, and D. Ponkratov, "Evaluation of cavitation erosion models on industrial maritime applications using commercial cfd software," in *Proceedings of the International Cavitation Symposium (CAV2024)*, International Cavitation Symposium, Jun. 2024.

[53] H. Xu, Z. Chen, Q. Wu, and Y. Cai, "A wall-modeled large-eddy simulation of the unsteady flow in a water-jet pump based on the turbulent length scales," *Ocean Engineering*, vol. 313, p. 119 559, 2024, ISSN: 0029-8018.

[54] P. Cao, Y. Wang, C. Kang, G. Li, and X. Zhang, "Investigation of the role of non-uniform suction flow in the performance of water-jet pump," *Ocean Engineering*, vol. 140, pp. 258–269, 2017, ISSN: 0029-8018.

[55] Z. Xu and H. Lai, "Comparison of cavitation in two axial-flow water jet propulsion pumps," *Processes*, 2023.

[56] B. Ji, Z.-y. Wang, H.-y. Cheng, and R. E. Bensow, "Cavitation research with computational fluid dynamics: From euler-euler to euler-lagrange approach," *Journal of Hydrodynamics*, vol. 36, pp. 1–23, 2024.

[57] Z. Wang, H. Cheng, R. E. Bensow, X. Peng, and B. Ji, "Numerical assessment of cavitation erosion risk on the delft twisted hydrofoil using a hybrid eulerian-lagrangian strategy," *International Journal of Mechanical Sciences*, vol. 259, p. 108 618, 2023, ISSN: 0020-7403.

[58] Y. Yang, C. Xiong, S. Wang, and A.-M. Zhang, "Cavitation erosion risk on a hydrofoil using a multi-scale method," *Physics of Fluids*, vol. 37, no. 2, p. 027 107, Feb. 2025, ISSN: 1070-6631.

[59] B. Budich, S. Schmidt, and N. Adams, "Numerical simulation of cavitating ship propeller flow and assessment of erosion aggressiveness," in *Proceedings of MARINE 2015 - Computational Methods in Marine Engineering VI*, CIMNE, Jun. 2015, pp. 709–721.

[60] A. Peters, U. Lantermann, and O. el Moctar, "Numerical prediction of cavitation erosion on a ship propeller in model- and full-scale," *Wear*, vol. 408-409, pp. 1–12, 2018, ISSN: 0043-1648.

[61] L. Kleinsorge, A. Peters, F. Schreiner, L. Greitsch, O. el Moctar, and R. Skoda, "Numerical prediction of cavitation erosion on ship propulsors," in *Proceedings of the 7th International Symposium on Marine Propulsors (smp'22)*, Wuxi, China, Jun. 2022, pp. 436–441.

[62] Z. Kaixuan, L. Yun, X. Qingjiang, X. Changjian, C. Jianping, and W. Dezhong, "Study on the experiment and numerical simulation of cavitation flow mechanisms at different flow rates in water-jet propulsion pumps," *Journal of Physics: Conference Series*, vol. 2707, no. 1, p. 012 050, Feb. 2024.

[63] M. Arabnejad, A. Eslamdoost, U. Svennberg, and R. Bensow, "Scale resolving simulations of the non-cavitating and cavitating flows in an axial water jet pump," in *33nd Symposium on Naval Hydrodynamics*, 2020, pp. 19–23.

[64] N. Qiu, H. Zhu, Y. Long, J. Zhong, R. Zhu, and S. Wu, "Assessment of cavitation erosion in a water-jet pump based on the erosive power method," *Scanning*, vol. 2021, 2021.

[65] ANSYS, Inc., *Ansys fluent theory guide*, 2021 R1 edition, Canonsburg, Pennsylvania, USA, 2021.

[66] Siemens Digital Industries Software, *Simcenter STAR-CCM+ User Guide v. 19.06-008*, version 19.06-008-r8, Siemens 2024.

[67] R. E. Bensow, "Simulation of the unsteady cavitation on the delft twist11 foil using rans, des and les," in *Second International Symposium on Marine Propulsors*, Hamburg, Germany, Jun. 2011.

[68] F. R. Menter, "Zonal two equation $k - \omega$ turbulence models for aerodynamic flows," in *24th Fluid Dynamics Conference*, Orlando, FL, Jul. 1993.

[69] J.-L. Reboud, B. Stutz, and O. Coutier, "Two-phase flow structure of cavitation: Experiment and modelling of unsteady effects," in *Proceedings of the 3rd International Symposium on Cavitation (CAV1998)*, Grenoble, France, Apr. 1998, pp. 1–8.

[70] F. Nicoud and F. Ducros, "Subgrid-scale stress modelling based on the square of the velocity gradient tensor," *Flow, Turbulence and Combustion*, vol. 62, no. 3, pp. 183–200, 1999.

[71] R. F.-P. O Coutier-Delgosha and J. L. Reboud, "Simulation of unsteady cavitation with a two-equation turbulence model including compressibility effects," *Journal of Turbulence*, vol. 3, N58, 2002.

[72] P. J. Zwart, A. G. Gerber, and T. Belamri, "A two-phase flow model for predicting cavitation dynamics," in *Fifth international conference on multiphase flow*, Yokohama Japan, vol. 152, 2004.

[73] G. H. Schnerr and J. Sauer, "Physical and numerical modeling of unsteady cavitation dynamics," in *Fourth international conference on multiphase flow*, ICMF New Orleans New Orleans, LO, USA, vol. 1, 2001, pp. 1–12.

[74] P. Koukouvinis, H. Naseri, and M. Gavaises, "Performance of turbulence and cavitation models in prediction of incipient and developed cavitation," *International Journal of Engine Research*, vol. 18, no. 4, pp. 333–350, 2017.

[75] J. Gross and G. Sadowski, "Perturbed-chain saft: An equation of state based on a perturbation theory for chain molecules," *Industrial & Engineering Chemistry Research*, vol. 40, no. 4, pp. 1244–1260, 2001.

[76] O. Lötgering-Lin and J. Gross, "Group contribution method for viscosities based on entropy scaling using the perturbed-chain polar statistical associating fluid theory," *Industrial & Engineering Chemistry Research*, vol. 54, no. 32, pp. 7942–7952, 2015.

[77] M. Hopp and J. Gross, "Thermal conductivity from entropy scaling: A group-contribution method," *Industrial & Engineering Chemistry Research*, vol. 58, pp. 20 441–20 449, 2019.

[78] E. Lemmon, M. Huber, and M. McLinden, *Nist standard reference database 23: Reference fluid thermodynamic and transport properties-refprop, version 9.1*, en, 2013-05-07 2013.

[79] A. Rubino, M. Pini, M. Kosec, S. Vitale, and P. Colonna, "A look-up table method based on unstructured grids and its application to non-ideal compressible fluid dynamic simulations," *Journal of Computational Science*, vol. 28, pp. 70–77, 2018, ISSN: 1877-7503.

[80] M. S. Mihatsch, S. J. Schmidt, M. Thalhamer, and N. A. Adams, "Numerical prediction of erosive collapse events in unsteady compressible cavitating flows," in *MARINE 2011, IV International Conference on Computational Methods in Marine Engineering: Selected Papers*. Dordrecht: Springer Netherlands, 2013, ch. 39, pp. 499–510, ISBN: 978-94-007-6143-8.

[81] GOM GmbH, *Gom inspect*, Version 2022, 2022.

[82] L. Davidson, "Large eddy simulations: How to evaluate resolution," *International Journal of Heat and Fluid Flow*, vol. 30, no. 5, pp. 1016–1025, 2009, The 3rd International Conference on Heat Transfer and Fluid Flow in Microscale, ISSN: 0142-727X.

[83] S. B. Pope, *Turbulent Flows*. Cambridge University Press, 2000.

[84] I. B. Celik, Z. N. Cehreli, and I. Yavuz, "Index of Resolution Quality for Large Eddy Simulations," *Journal of Fluids Engineering*, vol. 127, no. 5, pp. 949–958, Sep. 2005, ISSN: 0098-2202.

[85] B. Befrui, G. Corbinelli, D. Robart, W. Reckers, and H. Weller, "Les simulation of the internal flow and near-field spray structure of an outward-opening gdi injector and comparison with imaging data," in *SAE World Congress and Exhibition*, SAE International, Apr. 2008.